

FedLoDrop: Federated LoRA with Dropout for Generalized LLM Fine-tuning

Sijing Xie, Dingzhu Wen, Changsheng You, Qimei Chen, Mehdi Bennis, and Kaibin Huang

Abstract—Fine-tuning (FT) large language models (LLMs) is crucial for adapting general-purpose models to specific tasks, enhancing accuracy and relevance with minimal resources. To further enhance generalization ability while reducing training costs, this paper proposes Federated LoRA with Dropout (FedLoDrop), a new framework that applies dropout to the rows and columns of the trainable matrix in Federated LoRA. A generalization error bound and convergence analysis under sparsity regularization are obtained, which elucidate the fundamental trade-off between underfitting and overfitting. The error bound reveals that a higher dropout rate increases model sparsity, thereby lowering the upper bound of pointwise hypothesis stability (PHS). While this reduces the gap between empirical and generalization errors, it also incurs a higher empirical error, which, together with the gap, determines the overall generalization error. On the other hand, though dropout reduces communication costs, deploying FedLoDrop at the network edge still faces challenges due to limited network resources. To address this issue, an optimization problem is formulated to minimize the upper bound of the generalization error, by jointly optimizing the dropout rate and resource allocation subject to the latency and per-device energy consumption constraints. To solve this problem, a branch-and-bound (B&B)-based method is proposed to obtain its globally optimal solution. Moreover, to reduce the high computational complexity of the B&B-based method, a penalized successive convex approximation (P-SCA)-based algorithm is proposed to efficiently obtain its high-quality suboptimal solution. Finally, numerical results demonstrate the effectiveness of the proposed approach in mitigating overfitting and improving the generalization capability.

Index Terms—Large Language Models, Federated Learning, Low-rank Adaptation, Dropout, Generalization Error

I. INTRODUCTION

Recent developments in large language models (LLMs), such as ChatGPT, LLaMA, and Vision Transformers, have driven significant progress in artificial general intelligence (AGI) [1]. These models exhibit enhanced capabilities in generalization and inference. To adapt these models for specific tasks and data distributions, fine-tuning (FT) has become a key approach, which is crucial for establishing native artificial

S. Xie and D. Wen are with the School of Information Science and Technology, ShanghaiTech University, Shanghai 201210, China (e-mail: {xiesj2023, wendzh}@shanghaitech.edu.cn).

C. You is with the Department of Electronic and Electrical Engineering, Southern University of Science and Technology, Shenzhen 518055, China (e-mail: youcs@sustech.edu.cn).

Q. Chen is with the School of Electronic Information, Wuhan University, Wuhan 430072, China (e-mail: chenqimei@whu.edu.cn).

M. Bennis is with the Centre for Wireless Communications, University of Oulu, Oulu 90014, Finland (e-mail: mehdi.bennis@oulu.fi).

K. Huang is with the Department of Electrical and Electronic Engineering, The University of Hong Kong, Hong Kong SAR, China (e-mail: huangkb@eee.hku.hk).

intelligence (AI) in the era of 6G [2]–[4]. However, as model sizes grow, full-model FT becomes unaffordable in practice due to prohibitively high computational and memory costs.

To tackle these challenges, parameter-efficient fine-tuning (PEFT) has emerged as a pivotal approach [5]–[7]. PEFT updates only a small subset of model parameters, providing a balanced trade-off between computational efficiency and training performance. One notable method within PEFT is Low-Rank Adaptation (LoRA) [8], which employs low-rank matrices to approximate weight changes while keeping the original model weights frozen. The flexibility of LoRA allows it to be merged with the backbone, eliminating additional costs. Compared to other PEFT methods based on pruning, LoRA achieves superior efficiency-utility trade-offs [9]. The authors in [10] applied LoRA to a hierarchical LLM, classifying the instruction type and then utilizing task-specific networks to accomplish respective tasks. FT LLMs on a single device often result in suboptimal performance due to limited data and memory constraints [11]. Centralized FT faces significant challenges, mainly because of privacy concerns and regulatory restrictions on data access [12]. This is exacerbated by the fact that massive amounts of fragmented data are distributed across numerous devices at the network edge.

Federated learning (FL) enables privacy-preserving FT of pre-trained LLMs on distributed clients by sharing model updates between the server and clients, ensuring that distributed data remains localized [13]–[17]. This makes FL an appealing choice for aligning LLMs with specialized domains [18], [19]. Specifically, the authors in [20], [21] incorporated LoRA with FedAvg, significantly reducing the number of parameters that need to be synchronized across distributed devices. Several works have focused on improving the efficiency of federated LoRA. Due to the frequent exchange of LLM parameters among distributed devices, [9] proposed integrating communication compression with federated LoRA to further reduce the communication cost. In addition, a hierarchical FedLoRA framework was proposed in [22], which dynamically assigned diverse and suitable FT depths for each group, hence greatly reducing the computation and communication cost. The authors in [23] proposed a memory-efficient FT method, which sets the A matrices to fixed after initialization and trains only the B matrices. Other works focus on the deployment and performance of federated LoRA. [24] proposed an improved initialization strategy for LoRA’s weights, resulting in enhanced performance under the FedFM framework. Due to limited storage and computational capabilities at the edge devices, deploying the full model at edge devices is impractical. [25] presented a split federated LoRA framework, where

the computationally intensive encoder is deployed at the edge server, while others remain on edge devices.

However, one significant challenge when FT models on downstream tasks is overfitting. Simply reducing the rank of LoRA could help alleviate overfitting, but fewer learnable parameters indicate less expressive power, and might lead to suboptimal performances. AdaLoRA [26] optimizes LoRA by automatically pruning unimportant parameters with learned importance scores during training to prevent overfitting. However, this parameter selection method heavily relies on gradients of parameters on the training data, making the models less generalizable to unseen test data. To address this issue, a federated dropout framework was proposed in [27], which utilized the typical technique of dropout in deep learning. [28] further provided the convergence analysis for federated dropout, quantitatively showing the influence of dropout rate on convergence. In addition, the authors in [29] combined LoRA with dropout in an aggregation way. This, however, has the centralized challenges as mentioned before.

Towards this end, we propose a practical Federated LoRA with dropout (FedLoDrop) approach, which introduces random noise to the learnable low-rank matrices. FedLoDrop effectively mitigates overfitting while simultaneously reducing communication costs and minimizing update sizes transmitted from clients to the server¹. We provide the theoretical analysis using pointwise hypothesis stability (PHS) and Taylor expansion. Then, we aim to minimize the generalization error in each round by jointly optimizing dropout rate and network resource allocation. Finally, simulations are presented to validate the effectiveness of our proposed approach. The main contributions of this paper are listed below.

- **FedLoDrop Framework with Reduced Communication Cost:** We propose a practical FedLoDrop framework, where dropout is applied to the rows and columns of the tunable low-rank parameter matrices, e.g., \mathbf{A} and \mathbf{B} . Specifically, for device k with a dropout rate of $\gamma_k \in [0, 1]$, dropout technique deactivates neurons on the input and output sides of both trainable LoRA matrices [29]. After applying dropout, the communication overhead is scaled down to $(1 - \gamma)$ times of the original one.
- **Theoretical Analysis:** We characterize the effect of LoRA dropout on the sparsity and PHS upper bound. It is shown that a lower dropout rate enhances model complexity, increasing overfitting potential and widening the gap between generalization and empirical errors (adaptation function class). Conversely, a drastically high dropout rate may incur underfitting, significantly impairing the representation ability of the model and resulting in higher empirical error. This provides a theoretical foundation to balance the tradeoff between the adaptation function class and empirical error. Moreover, a convergence analysis

¹Mixture-of-Experts (MoE) has recently emerged as an effective paradigm for reducing computational overhead and can serve as a complementary approach to FedLoDrop. The adaptive dropout mechanisms in FedLoDrop could be specifically tailored to promote more balanced expert utilization across heterogeneous clients, thereby preventing any single expert from dominating the learning process or remaining underutilized.

is also conducted, revealing that the convergence rate becomes slower with increasing dropout rate.

- **Joint Dropout Control and Resource Allocation:** Based on the theoretical analysis for FedLoDrop, we formulate an optimization problem to minimize the generalization error of each FT round under the network resource constraint, which is shown to be dependent on the dropout rate of each device. Particularly, a larger dropout rate leads to a smaller gap between empirical and generalization errors. As the exact form of the learning loss reduction in the generalization error bound is intractable, its upper bound is minimized instead without loss of generality, under the constraints of limited system subcarriers, completion latency, and per-device energy consumption. A branch-and-bound (B&B)-based method is proposed to find the globally optimal solution. Moreover, to efficiently solve the problem, a low-complexity penalized successive convex approximation (P-SCA)-based solution is proposed to find a high-quality suboptimal solution.

- **Performance Evaluation:** Extensive simulations based on multi-language tasks are conducted to evaluate the performance of the proposed schemes. We mainly FT two LLMs, RoBERTa-large (355M) and LLaMA (7B), on the GLUE and MMLU benchmarks, respectively. With dropout, the generalization ability of the fine-tuned model is significantly improved, thus enabling the capability to effectively apply the knowledge from the FT dataset to natural language response tasks. In both scenarios, more network resources, i.e., a longer latency, allow lower dropout rates of all devices, leading to improved testing performance.

II. FRAMEWORK OF FEDERATED LORA DROPOUT

A. Preliminary LoRA

LoRA fine-tunes LLMs efficiently by maintaining the original model weights $\boldsymbol{\theta}_0$ frozen and adding low-rank trainable matrices [8]. Specifically, the loss function of an LLM in the FT stage is $\mathcal{L} = \frac{1}{|\mathcal{D}|} \sum_{i \in \mathcal{D}} \ell(\Delta\boldsymbol{\theta}; \boldsymbol{\theta}_0, \mathbf{x}_i)$, where \mathcal{D} is the dataset, $|\mathcal{D}|$ is the size of dataset, \mathbf{x}_i is the i -th data sample therein, and $\ell(\cdot; \cdot)$ is the empirical loss function that characterizes the difference between the output and real label.

Consider an arbitrary layer in an arbitrary training round $\mathbf{W}_{u,t}$ applied with LoRA for FT, a LoRA update is thus characterized by a set of low-rank trainable weights $\Delta\boldsymbol{\theta}_t \triangleq \{\Delta\mathbf{W}_{u,t}\}_{u=1}^{U'}$, a set of pre-trained weight $\boldsymbol{\theta}_0 \triangleq \{\mathbf{W}_{u,0}\}_{u=1}^U$, where U' is the number of weight matrices applying LoRA and U is the number of all matrices. LoRA may not update all matrices, in which case $U' \leq U$. The parameter matrix $\mathbf{W}_{u,t} \in \mathbb{R}^{n_1 \times n_2}$ can be regarded as the sum of a frozen pre-trained matrix $\mathbf{W}_{u,0} \in \mathbb{R}^{n_1 \times n_2}$ and a trainable low-rank decomposable matrix $\Delta\mathbf{W}_{u,t} \in \mathbb{R}^{n_1 \times n_2}$, i.e.,

$$\mathbf{W}_{u,t} = \mathbf{W}_{u,0} + \Delta\mathbf{W}_{u,t} = \mathbf{W}_{u,0} + \mathbf{B}_{u,t}\mathbf{A}_{u,t}, \quad (1)$$

where $\mathbf{A}_{u,t} \in \mathbb{R}^{r \times n_2}$ and $\mathbf{B}_{u,t} \in \mathbb{R}^{n_1 \times r}$ are trainable low-rank matrices, with $r \ll \{n_1, n_2\}$. For an arbitrary training round t and data sample i , the training procedure of LoRA is presented below.

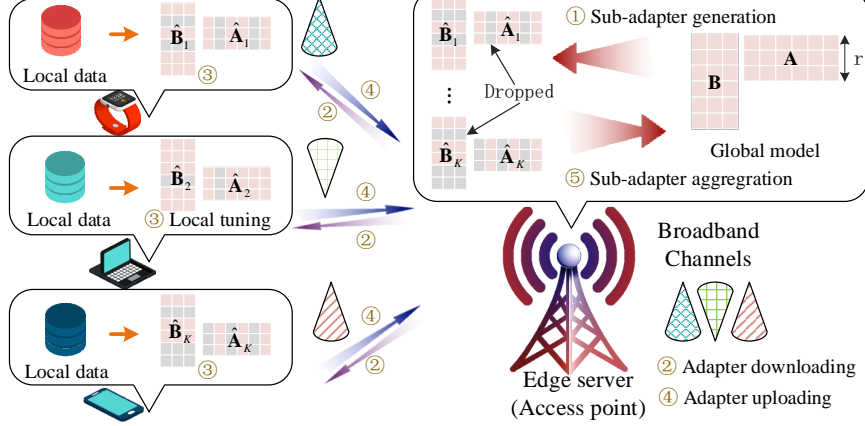


Fig. 1. The operations of FedLoDrop in a wireless system.

1) *Forward Pass*: The output of the u -th layer is given by

$$\begin{aligned} \mathbf{h}_{u,i,t} &= \mathbf{W}_{u,t-1} \mathbf{f}_{u-1,i,t} = (\mathbf{W}_{u,0} + \Delta \mathbf{W}_{u,t-1}) \mathbf{f}_{u-1,i,t} \\ &= (\mathbf{W}_{u,0} + \mathbf{B}_{u,t-1} \mathbf{A}_{u,t-1}) \mathbf{f}_{u-1,i,t}, \end{aligned} \quad (2)$$

where $\mathbf{f}_{u-1,i,t}$ is the output of the previous layer.

2) *Backward Pass*: During the backward propagation, the stochastic gradients of the two low-rank matrices \mathbf{B} and \mathbf{A} are calculated individually, given by

$$\begin{aligned} \Delta \mathbf{B}_{u,i,t-1} &= \frac{\partial \ell_t}{\partial \mathbf{B}_{u,t-1}} = \frac{\partial \ell_t}{\partial \mathbf{h}_{u,i,t}} \frac{\partial \mathbf{h}_{u,i,t}}{\partial \mathbf{B}_{u,t-1}} \\ &= \frac{\partial \ell_t}{\partial \mathbf{h}_{u,i,t}} \cdot (\mathbf{A}_{u,t-1} \mathbf{f}_{u-1,i,t})^\top, \end{aligned} \quad (3)$$

$$\begin{aligned} \Delta \mathbf{A}_{u,i,t-1} &= \frac{\partial \ell_t}{\partial \mathbf{A}_{u,t-1}} = \frac{\partial \ell_t}{\partial \mathbf{h}_{u,i,t}} \frac{\partial \mathbf{h}_{u,i,t}}{\partial \mathbf{A}_{u,t-1}} \\ &= \mathbf{B}_{u,t-1}^\top \cdot \frac{\partial \ell_t}{\partial \mathbf{h}_{u,i,t}} \cdot \mathbf{f}_{u-1,i,t}^\top. \end{aligned} \quad (4)$$

3) *Low-rank Matrices Updating*: $\mathbf{B}_{u,t}$ and $\mathbf{A}_{u,t}$ are updated by the aggregated stochastic gradients of all data samples [29]–[31], i.e.,

$$\begin{aligned} \Delta \mathbf{B}_{u,t-1} &= \frac{\partial \mathcal{L}}{\partial \mathbf{B}_{u,t-1}} = \frac{1}{|\mathcal{D}|} \sum_{i \in \mathcal{D}} \frac{\partial \ell_t}{\partial \mathbf{B}_{u,t-1}} \\ &= \frac{1}{|\mathcal{D}|} \sum_{i \in \mathcal{D}} \Delta \mathbf{B}_{u,i,t-1}, \end{aligned} \quad (5)$$

$$\begin{aligned} \Delta \mathbf{A}_{u,t-1} &= \frac{\partial \mathcal{L}}{\partial \mathbf{A}_{u,t-1}} = \frac{1}{|\mathcal{D}|} \sum_{i \in \mathcal{D}} \frac{\partial \ell_t}{\partial \mathbf{A}_{u,t-1}} \\ &= \frac{1}{|\mathcal{D}|} \sum_{i \in \mathcal{D}} \Delta \mathbf{A}_{u,i,t-1}, \end{aligned} \quad (6)$$

where $\Delta \mathbf{B}_{u,i,t-1}$ and $\Delta \mathbf{A}_{u,i,t-1}$ are the sample-wise stochastic gradient matrices of the u -th layer defined in (3), (4). Then $\mathbf{B}_{u,t}$ and $\mathbf{A}_{u,t}$ are updated through gradient descent, with α_B and α_A being the learning rate:

$$\mathbf{B}_{u,t} = \mathbf{B}_{u,t-1} - \alpha_B \Delta \mathbf{B}_{u,t-1}, \quad (7)$$

$$\mathbf{A}_{u,t} = \mathbf{A}_{u,t-1} - \alpha_A \Delta \mathbf{A}_{u,t-1}. \quad (8)$$

Next, the trainable matrix $\Delta \mathbf{W}_{u,t}$ is updated by

$$\Delta \mathbf{W}_{u,t} = \mathbf{B}_{u,t} \mathbf{A}_{u,t}, \quad (9)$$

and the parameter matrix $\mathbf{W}_{u,t}$ is updated by

$$\mathbf{W}_{u,t} = \mathbf{W}_{u,0} + \Delta \mathbf{W}_{u,t}. \quad (10)$$

Remark 1. The low-rank matrices updating method presented in (5) – (9) is not equivalent to the sample average of the updates of $\Delta \mathbf{W}_u$, i.e.,

$$\begin{aligned} \Delta \mathbf{W}_{u,t} &= \left(\mathbf{B}_{u,t-1} - \frac{\alpha_B}{|\mathcal{D}|} \sum_{i \in \mathcal{D}} \Delta \mathbf{B}_{u,i,t-1} \right) \\ &\quad \left(\mathbf{A}_{u,t-1} - \frac{\alpha_A}{|\mathcal{D}|} \sum_{i \in \mathcal{D}} \Delta \mathbf{A}_{u,i,t-1} \right) \\ &\neq \frac{1}{|\mathcal{D}|} \sum_{i \in \mathcal{D}} (\mathbf{B}_{u,t-1} - \alpha_B \Delta \mathbf{B}_{u,i,t-1}) \\ &\quad (\mathbf{A}_{u,t-1} - \alpha_A \Delta \mathbf{A}_{u,i,t-1}). \end{aligned}$$

However, this enjoys two benefits. On one hand, it simplifies the initialization of \mathbf{B} and \mathbf{A} by utilizing the ones in the last training round. On the other hand, this approach is well-suited for distributed implementations [20], [24]. In each round, devices only need to transmit $\mathbf{B}_{u,t-1}$ and $\mathbf{A}_{u,t-1}$, which have a lower dimensionality compared to $\Delta \mathbf{W}_{u,t-1}$, thereby reducing the communication overhead.

B. LoRA Dropout

The original dropout technique was proposed in [32] to avoid overfitting during training. In standard dropout, each neuron in the network is dropped from the network with a certain probability. Given that dropout techniques have proven effective in controlling overfitting, we introduce a LoRA dropout framework to enhance generalization when adapting to downstream tasks. The loss function can be re-written as $\mathcal{L} = \frac{1}{|\mathcal{D}|} \sum_{i \in \mathcal{D}} \ell(\Delta \theta(\mathbf{m}_t); \theta_0, x_i)$, where $\Delta \theta(\mathbf{m}_t)$ is the LoRA parameters after the dropout, \mathbf{m}_t is the concatenation of masks of all LoRA modules, which varies in different training rounds, and θ_0 is the original parameters of the pre-trained model.

As shown step ① in Fig. 1, for a LoRA module, rows and columns are randomly dropped from both tunable low-rank parameter matrices with a probability of γ_t , which is called dropout rate. In other words, LoRA dropout strategy samples random neurons on the input and output sides of LoRA matrices with a probability γ_t to mask them to zeros [29]. Thereby, the low-rank matrices after dropout are given by

$$\begin{cases} \hat{\mathbf{A}}_{u,t} = \mathbf{A}_{u,t} \cdot \text{diag}(\mathbf{m}_{A,t}), \mathbf{m}_{A,t} \sim \text{Bern}(1 - \gamma_t), \\ \hat{\mathbf{B}}_{u,t} = (\mathbf{B}_{u,t}^\top \cdot \text{diag}(\mathbf{m}_{B,t}))^\top, \mathbf{m}_{B,t} \sim \text{Bern}(1 - \gamma_t), \end{cases} \quad (11)$$

where $\mathbf{m}_{A,t} \in \mathbb{R}^{n_2}$, $\mathbf{m}_{B,t} \in \mathbb{R}^{n_1}$, $\text{Bern}(1 - \gamma_t)$ means that all elements of a matrix are independently distributed as the identical Bernoulli distribution with parameter $(1 - \gamma_t)$. With dropout, the sizes of $\hat{\mathbf{A}}_{u,t}$ and $\hat{\mathbf{B}}_{u,t}$ are further reduced. In the t -th training round, for the i -th data sample, the training procedure is presented below.

1) *Forward Pass*: After dropout, the output of the u -th layer is given by

$$\hat{\mathbf{h}}_{u,i,t} = (\mathbf{W}_{u,0} + \hat{\mathbf{B}}_{u,t-1} \hat{\mathbf{A}}_{u,t-1}) \mathbf{f}_{u-1,i,t}. \quad (12)$$

2) *Backward Pass and Low-rank Matrices Updating*:

During backpropagation, the stochastic gradients of $\hat{\mathbf{B}}_{u,t}$ and $\hat{\mathbf{A}}_{u,t}$ are computed according to (5), (6) and updated following (7), (8). Notably, the dropped parameters will not be updated, thereby reducing the computational overhead. After obtaining $\hat{\mathbf{B}}_{u,t}$ and $\hat{\mathbf{A}}_{u,t}$, the matrices $\Delta\hat{\mathbf{W}}_{u,t}$ and $\hat{\mathbf{W}}_{u,t}$ are calculated in the same manner as (9) and (10).

C. Federated LoRA with Dropout

1) *Procedure and Algorithm*: In this case, each device k holds a local dataset, denoted by $\mathcal{D}_k = \{\mathbf{x}_i | i = 1, 2, \dots, |\mathcal{D}_k|\}$, where \mathbf{x}_i is the i -th data sample and the size of \mathcal{D}_k is $|\mathcal{D}_k|$. Denote $\Delta\theta(\mathbf{m}_{k,t})$ as the LoRA parameters after the dropout for the k -th device, $\mathbf{m}_{k,t}$ as the concatenation of all dropout masks of LoRA modules, which varies across different training rounds and different devices, and θ_0 as the original parameters of the pre-trained model, which has been stored in each device in advance. The objective is to minimize the global loss function, given by $\mathcal{L} = \sum_{k=1}^K \frac{|\mathcal{D}_k|}{|\mathcal{D}|} \ell_k(\Delta\theta(\mathbf{m}_{k,t}); \theta_0, \mathcal{D}_k)$, where $\mathcal{D} = \{\mathcal{D}_k\}$ is the global dataset, the local loss function of the k -th device can be written as $\ell_k(\Delta\theta(\mathbf{m}_{k,t}); \theta_0, \mathcal{D}_k) = \frac{1}{|\mathcal{D}_k|} \sum_{x_i \in \mathcal{D}_k} \ell_{k,i}(\Delta\theta(\mathbf{m}_{k,t}); \theta_0, \mathbf{x}_i)$. Similar to (11), FedLoDrop can be written as

$$\begin{aligned} \hat{\mathbf{A}}_{u,k,t} &= \mathbf{A}_{u,t} \cdot \text{diag}(\mathbf{m}_{k,A,t}), \mathbf{m}_{k,A,t} \sim \text{Bern}(1 - \gamma_{k,t}), \\ \hat{\mathbf{B}}_{u,k,t} &= (\mathbf{B}_{u,t}^\top \cdot \text{diag}(\mathbf{m}_{k,B,t}))^\top, \mathbf{m}_{k,B,t} \sim \text{Bern}(1 - \gamma_{k,t}), \end{aligned} \quad (13)$$

The forward and backward pass on each device has minor changes to the aforementioned situations and thus are omitted.

As illustrated in Fig. 1 and Algorithm 1, the overall framework involves two primary components: local tuning operations on the client side, and dropout and aggregation operations on the server side, which work together to ensure efficient training. There are five steps to complete an arbitrary training round t , as described below.

- *LoRA Sub-adapter Generation*: The server adopts the LoRA dropout technique introduced in Section II-B to generate a sub-adapter for each device.
- *Adapter Downloading*: Each device downloads its corresponding sub-adapter $\hat{\mathbf{B}}_{k,t}$ and $\hat{\mathbf{A}}_{k,t}$ from the server, where $\hat{\mathbf{B}}_{k,t} \triangleq \{\hat{\mathbf{B}}_{u,k,t}\}_{u=1}^{U'}$, $\hat{\mathbf{A}}_{k,t} \triangleq \{\hat{\mathbf{A}}_{u,k,t}\}_{u=1}^{U'}$.
- *Client Local Tuning*: Each device first calculates the product of two low-rank adapters and updates them based on pre-trained model and its own datasets, as shown in (5) – (8).
- *Adapter Uploading*: Each device uploads the updated gradients of local sub-adapters to the server by the allocated subcarriers.
- *Server Aggregation*: The server reconstructs the full-size adapter update via zero-padding: it inserts zeros into the dropped positions. This process is feasible because the server has knowledge of the sparsity mask. Then, all complete networks are aggregated for updating the global network, expressed as:

$$\begin{aligned} \mathbf{B}_t &= \mathbf{B}_{t-1} - \alpha_B \sum_{k=1}^K \frac{|\mathcal{D}_k|}{|\mathcal{D}|} \Delta\hat{\mathbf{B}}_{k,t-1} \\ &= \mathbf{B}_{t-1} - \alpha_B \Delta\hat{\mathbf{B}}_{t-1}, \end{aligned} \quad (14)$$

$$\begin{aligned} \mathbf{A}_t &= \mathbf{A}_{t-1} - \alpha_A \sum_{k=1}^K \frac{|\mathcal{D}_k|}{|\mathcal{D}|} \Delta\hat{\mathbf{A}}_{k,t-1} \\ &= \mathbf{A}_{t-1} - \alpha_A \Delta\hat{\mathbf{A}}_{t-1}. \end{aligned} \quad (15)$$

Remark 2. Combined with LoRA dropout, the inference caused by the cross-product of sub-adapters from different clients can be diminished. Furthermore, FedLoDrop inherently provides a degree of privacy due to the sparsification of transmitted updates against potential privacy attacks such as gradient inversion or model extraction. That said, the dropout-based sparsification in FedLoDrop may offer incidental protection against gradient inversion attacks, as partially masked updates reduce the amount of information available to an adversary. Similarly, the local gradient tracking mechanism further decouples client-specific information from the global model, potentially mitigating model extraction risks.

2) *Communication-computation-memory Overhead*:

- *Communication overhead*: FedLoDrop provides significant competitive savings at both uploading and downloading links. In round t , each device downloads and uploads $\hat{\mathbf{B}}_{k,t}$ and $\hat{\mathbf{A}}_{k,t}$ to the server for aggregation. The original number of transmitted parameters is $M = (n_1 + n_2)r$. After applying dropout, with a dropout rate of $\gamma_k \in [0, 1]$ for device k , the communication overhead becomes $\hat{M}_{k,t} = (1 - \gamma_{k,t})(n_1 + n_2)r = (1 - \gamma_{k,t})M$.
- *Computation and memory overhead*: FedLoDrop saves local computation workloads and memory cost by maintaining sparse adapters throughout the FL process. No part of FedLoDrop requires dense training, and the computation overhead is conducted sample-wise. As the computation and memory costs of adapters are small compared to the costs of the backbone and dropout only

Algorithm 1: The training process of FedLoDrop

Parameters: Communication round T ; The pre-trained model \mathbf{W}_0 ; The local trainable and efficient parameters \mathbf{B}_k , \mathbf{A}_k and the local dataset \mathcal{D}_k of the k -th device.

Before Training: Store \mathbf{W}_0 on each device, and initialize \mathbf{B}_0 , and \mathbf{A}_0 on the server.

Server executes:

for each communication round $t = 1$ to T **do**
 $\hat{\mathbf{B}}_{k,t-1}$, $\hat{\mathbf{A}}_{k,t-1} \leftarrow$ (LoRA dropout)
Send $\hat{\mathbf{B}}_{k,t-1}$, $\hat{\mathbf{A}}_{k,t-1}$ to each device
for each device **in parallel do**
| ClientLocalTuning (k , $\hat{\mathbf{B}}_{k,t-1}$, $\hat{\mathbf{A}}_{k,t-1}$)
end
Receive local updated parameters
Global Aggregation by zero padding and (14), (15)
end

ClientLocalTuning (k , $\hat{\mathbf{B}}_{k,t-1}$, $\hat{\mathbf{A}}_{k,t-1}$):
 $\hat{\mathbf{B}}_{k,t}$, $\hat{\mathbf{A}}_{k,t} \leftarrow$ (5) – (8)
Send updated parameters to the server

reduces computation overhead in backward propagation, the computation and memory benefits are omitted [9].

III. THEORETICAL ANALYSIS

In the FT phase, we first formulate an optimization problem to minimize the loss function under the constraint of model sparsity. Subsequently, we characterize a generalization error bound within the framework of sparsity regularization, which demonstrates a fundamental trade-off between underfitting and overfitting in the context of LoRA dropout. Next, the upper bounding loss descent is formulated. Finally, the convergence of FedLoDrop is performed.

A. LoRA Dropout FT Through Sparse Regularization

Building upon the LoRA dropout mechanism presented on a single device by [29], we extend this framework to accommodate FL environments. Assume $\mathbf{d}_{k,t} \in \{0, 1\}$ as a dropout instance applied to the production of LoRA matrices, i.e., $\mathbf{d}_{k,t} \sim \text{Bern}(1 - (1 - \gamma_{k,t})^2)$, namely, $\mathbf{d}_{k,t} \sim \text{Bern}(2\gamma_{k,t} - \gamma_{k,t}^2)$, where $\mathbf{d}_{k,t}$ equals to one when the corresponding entry is dropped to zero and set as zero otherwise. The FT to minimize the loss function can be formulated as:

$$\begin{aligned} & \min_{\{\Delta\theta_{k,t}\}} \sum_{k=1}^K \frac{|\mathcal{D}_k|}{|\mathcal{D}|} \ell_k(\Delta\theta_{k,t}; \theta_0, \mathcal{D}_k), \\ & \text{subject to } \mathbb{E}_{\mathbf{d}_{k,t} \sim \text{Bern}(2\gamma_{k,t} - \gamma_{k,t}^2)} \|\mathbf{d}_{k,t} \odot \Delta\theta_{k,t}\|_2^2 \leq c, \forall k, \end{aligned} \quad (16)$$

where c is a constant, and the condition denotes the sparsity of $\Delta\theta_{k,t}$. The regularized optimization problem of the global one is

$$\begin{aligned} \mathcal{L}'_{\{\nu_{k,t}\}} &= \sum_{k=1}^K \frac{|\mathcal{D}_k|}{|\mathcal{D}|} \left(\min_{\{\Delta\theta_{k,t}\}} \ell_k(\Delta\theta_{k,t}; \theta_0, \mathcal{D}_k) + \right. \\ & \left. \sum_{k=1}^K \nu_{k,t} \mathbb{E}_{\mathbf{d}_{k,t} \sim \text{Bern}(2\gamma_{k,t} - \gamma_{k,t}^2)} \|\mathbf{d}_{k,t} \odot \Delta\theta_{k,t}\|_2^2 \right) = \sum_{k=1}^K \frac{|\mathcal{D}_k|}{|\mathcal{D}|} \ell_{k,\lambda_t}, \end{aligned} \quad (17)$$

where $\ell_{k,\lambda_t} = \min_{\{\Delta\theta_{k,t}\}} \ell_k(\Delta\theta_{k,t}; \theta_0, \mathcal{D}_k) + \lambda_t \mathbb{E}_{\mathbf{d}_{k,t} \sim \text{Bern}(2\gamma_{k,t} - \gamma_{k,t}^2)} \|\mathbf{d}_{k,t} \odot \Delta\theta_{k,t}\|_2^2$ is the regularized optimization problem for each device. $\nu_{k,t}$, λ_t are arbitrary hyper-parameter.

B. Generalization Error Analysis

The stability of the sparse-regularized algorithm is analyzed to assess the generalization error bound of LoRA dropout FT by optimizing ℓ_{k,λ_t} . Stability is a well-explored subject in machine learning [33], [34] and we adopt a utilized analytical framework, pointwise hypothesis stability (PHS)[35]. This approach examines the perturbation of the optimal model when a single training sample is removed. For each device, the entire training dataset is \mathcal{D}_k , and the dataset after removing a sample \mathbf{x}_j as $\mathcal{D}_k^j = \mathcal{D}_k - \{\mathbf{x}_j\}$. It is assumed that $j \sim U(|\mathcal{D}_k|)$, which means the removal is sampled from a uniform distribution. $\theta_\ell(\mathcal{D}_k)$ is defined as the optimal model parameters with respect to (w.r.t.) loss function ℓ and dataset \mathcal{D}_k .

Definition 1. A learning algorithm parameterized by θ w.r.t. a loss function ℓ has PHS β , if:

$$\mathbb{E}_{\mathcal{D}_k, j \sim U(n)} \left| \ell(\theta_\ell(\mathcal{D}_k^j), \mathbf{x}_j) - \ell(\theta_\ell(\mathcal{D}_k), \mathbf{x}_j) \right| \leq \beta. \quad (18)$$

In (18), $\ell(\theta, \mathbf{x}_j)$ represents the loss for sample \mathbf{x}_j given model parameters θ . According to [29], if the following requirements are met: ℓ is η -Lipschitz, $\theta_{\ell_{k,\lambda_t}}(\mathcal{D}_k)$ is close to $\theta_{\ell_{k,\lambda_t}}(\mathcal{D}_k^j)$, Hessian matrix $\nabla^2 \ell_{k,\lambda_t}(\theta_{\ell_{k,\lambda_t}}(\mathcal{D}_k))$ at $\theta_{\ell_{k,\lambda_t}}(\mathcal{D}_k)$ is positive-semidefinite with a singular value decomposition $U_{k,t} \text{diag}(\Lambda_{k,t}) U_{k,t}^{-1}$, and $\Lambda_{k,t,\min} = \min\{\Lambda_{k,t,1}, \dots, \Lambda_{k,t,m}\}$, then the LoRA dropout algorithm optimizing ℓ_{k,λ_t} on $|\mathcal{D}_k|$ has an upper bound of PHS of ²

$$\begin{aligned} & \mathbb{E}_{\mathcal{D}_k, j \sim U(n)} \left| \ell_{k,\lambda_t}(\theta_{\ell_{k,\lambda_t}}(\mathcal{D}_k^j), \mathbf{x}_j) - \ell_{k,\lambda_t}(\theta_{\ell_{k,\lambda_t}}(\mathcal{D}_k), \mathbf{x}_j) \right| \\ & \leq \frac{2\eta^2}{(\Lambda_{k,t,\min} + 2\lambda_t(2\gamma_{k,t} - \gamma_{k,t}^2)) |\mathcal{D}_k|}. \end{aligned} \quad (19)$$

Theorem 1. If the conditions in Definition 1 are met (i.e., (18)), PHS of LoRA dropout algorithm on each device can be upper-bounded as

$$\begin{aligned} & \mathbb{E}_{\mathcal{D}_k, j \sim U(n)} \left| \ell_{k,\lambda_t}(\theta_{\ell_{k,\lambda_t}}(\mathcal{D}_k^j), \mathbf{x}_j) - \ell_{k,\lambda_t}(\theta_{\ell_{k,\lambda_t}}(\mathcal{D}_k), \mathbf{x}_j) \right| \\ & \leq \frac{2\eta^2}{(\Lambda_{k,t,\min} + 2\lambda_t(2\gamma_{k,t} - \gamma_{k,t}^2)) |\mathcal{D}_k|}. \end{aligned} \quad (20)$$

²We only require the regularization coefficient to be sufficiently large (i.e., $\lambda_t \geq \frac{1}{2} \Lambda_{k,t,\min}$), avoiding overly strong assumptions on the objective function. Since uniform stability is stricter and argument stability focuses on parameters, we adopt PHS. Despite the non-convexity of LLM training, which may introduce theoretical gaps, the resulting bound provides meaningful qualitative insights into the client numbers and dropout rates. Tighter bounds under weaker assumptions remain an exciting direction for future work.

Proof. Please refer to Appendix A. \square

Theorem 2. Based on the relation in (17), PHS of LoRA dropout algorithm on the server can be upper-bounded as

$$\begin{aligned} & \mathbb{E}_{\mathcal{D}, j \sim U(n)} \left| \mathcal{L}'_{\{\nu_{k,t}\}} \left(\boldsymbol{\theta}_{\mathcal{L}'_{\{\nu_{k,t}\}}}(\mathcal{D}^{\{j\}}), \mathbf{x}_{\{j\}} \right) \right. \\ & \quad \left. - \mathcal{L}'_{\{\nu_{k,t}\}} \left(\boldsymbol{\theta}_{\mathcal{L}'_{\{\nu_{k,t}\}}}(\mathcal{D}), \mathbf{x}_{\{j\}} \right) \right| \quad (21) \\ & \leq \sum_{k=1}^K \frac{2\eta^2}{(\Lambda_{k,t,\min} + 2\lambda_t(2\gamma_{k,t} - \gamma_{k,t}^2))|\mathcal{D}|}. \end{aligned}$$

It follows from Theorem 2 that increasing dropout rates (enhancing sparsity) leads to a reduction in the upper bound, indicating that sparser models exhibit greater stability. Consequently, with established stability bounds, the generalization error for the sparse fine-tuned model can be determined.

Lemma 1. For any learning algorithm \mathbb{M} having parameter W and bounded loss function ℓ satisfying $0 \leq |\ell(x) - \ell(x')| \leq C, \forall x, x'$. If \mathbb{M} has a PHS β , with probability $1 - \delta$, we have:

$$R(\mathbb{M}, \mathcal{D}) \leq \hat{R}(\mathbb{M}, \mathcal{D}) + \sqrt{\frac{C^2 + 12C|\mathcal{D}|\beta}{2|\mathcal{D}|\delta}}, \quad (22)$$

where $R(\mathbb{M}, \mathcal{D}) = \sum_k \frac{|\mathcal{D}_k|}{|\mathcal{D}|} \mathbb{E}[\ell_k(\boldsymbol{\theta}, |\mathcal{D}_k|)]$ and $\hat{R}(\mathbb{M}, \mathcal{D}) = \sum_k \frac{|\mathcal{D}_k|}{|\mathcal{D}|} \ell_k(\boldsymbol{\theta}, |\mathcal{D}_k|)$ denote the generalization risk and empirical risk of algorithm \mathbb{M} running on dataset \mathcal{D} , respectively.

Theorem 3. In training round t , given a LoRA dropout rate $\gamma_{k,t}$ and sparsity regularization λ_t , if the conditions in Definition 1 are met (i.e., (18)), then for some constant C , with probability $1 - \delta$,

$$\begin{aligned} R(M, \mathcal{D}) & \leq \hat{R}(M, \mathcal{D}) \\ & + \sqrt{\frac{C^2 + \sum_{k=1}^K \frac{24C\eta^2}{\Lambda_{k,t,\min} + 2\lambda_t(2\gamma_{k,t} - \gamma_{k,t}^2)}}{2|\mathcal{D}|\delta}}. \quad (23) \end{aligned}$$

Theorem 3 elucidates the connection between generalization error and dropout rate. It is shown that increasing the dropout rate decreases the gap between empirical and generalization errors but concurrently increases empirical error. Therefore, an appropriate dropout rate would help balance a trade-off between overfitting and underfitting. A larger value of λ_t more strongly enforces the sparsity constraint, resulting in a more compact parameter update and a lower theoretical generalization error bound. This, in turn, reduces the risk of overfitting and enhances the model's expected performance on unseen data. While the theorem does not explicitly characterize the relationship between generalization error and LoRA rank, it suggests that decreasing the rank-enhancing parameter sparsity-typically correlates with reduced generalization error. This implies that a model with a lower effective rank tends to have better generalization performance [35].

C. Upper Bounding Loss Descent

However, since $\hat{R}(M, \mathcal{D})$ lacks an analytical expression, the problem is not directly solvable. To address this, upper bounds for $\hat{R}(M, \mathcal{D})$ is derived. Without loss of generality,

the following assumptions are made [36], [37]. We assume a constant batch size and learning rate in the following analysis.

Assumption 1 (Lipschitz Continuous Gradient). $\nabla \mathcal{L}(\Delta \boldsymbol{\theta})$ is Lipschitz continuous with $\eta > 0$ such that, $\|\nabla \mathcal{L}(\Delta \boldsymbol{\theta}_2) - \nabla \mathcal{L}(\Delta \boldsymbol{\theta}_1)\|_F \leq \eta \|\Delta \boldsymbol{\theta}_2 - \Delta \boldsymbol{\theta}_1\|_F$, where $\|\cdot\|_F$ calculates the Frobenius-norm (F-norm).

Assumption 2 (Bounded Gradient Matrix). The F-norm of gradient matrix is upper bounded, i.e., $\mathbb{E}[\|\mathbf{H}(\cdot)\|_F^2] \leq \mathcal{H}^2$.

Assumption 3 (Small Dropout Rate). The dropout rate of each device is small so that the higher-order terms can be ignored.

Assumption 4 (Bounded weight). The F-norm of the parameter vector is upper bounded, i.e., $\mathbb{E}[\|\mathbf{A}_t\|_F^2], \mathbb{E}[\|\mathbf{B}_t\|_F^2] \leq \mathcal{G}^2, \forall k, t$.

Assumption 5 (Polyak-Łojaciewicz inequality). Optimal loss function value of \mathcal{L} exists, denoted \mathcal{L}^* , a constant $\mu \geq 0$ exists, and $\rho = \mathcal{L}(\Delta \boldsymbol{\theta}) - \mathcal{L}^*$ that satisfies $\|\nabla \mathcal{L}(\Delta \boldsymbol{\theta})\|_F^2 \geq 2\mu\rho$.

Specifically, it has been proven in [36], [37] that the transformer-based LLM possesses a Lipschitz continuous gradient, satisfying Assumption 1. The PL Assumption 5 is weaker than strong convexity, and usually considered in the analysis of non-convex cases.

Lemma 2. Similar to [37], the update of $\Delta \mathbf{W}_{u,t}$ can be expressed as

$$\begin{aligned} \Delta \mathbf{W}_{u,t} &= \mathbf{B}_{u,t} \mathbf{A}_{u,t} \\ &= (\mathbf{B}_{u,t-1} - \alpha_B \Delta \hat{\mathbf{B}}_{u,t-1})(\mathbf{A}_{u,t-1} - \alpha_A \Delta \hat{\mathbf{A}}_{u,t-1}) \\ &\stackrel{(a)}{\approx} \mathbf{B}_{u,t-1} \mathbf{A}_{u,t-1} - \alpha_A \mathbf{B}_{u,t-1} \Delta \hat{\mathbf{A}}_{u,t-1} \\ &\quad - \alpha_B \Delta \hat{\mathbf{B}}_{u,t-1} \mathbf{A}_{u,t-1} \\ &\stackrel{(b)}{=} \Delta \mathbf{W}_{u,t-1} - \alpha(\mathbf{B}_{u,t-1} \Delta \hat{\mathbf{A}}_{u,t-1} + \Delta \hat{\mathbf{B}}_{u,t-1} \mathbf{A}_{u,t-1}) \\ &\stackrel{(c)}{=} \Delta \mathbf{W}_{u,t-1} - \alpha(\mathbf{G}_{u,t-1} - \mathbf{J}_{u,t-1}), \quad (24) \end{aligned}$$

where (a) comes from the slight term of the gradient matrices product caused by the $\alpha_A \alpha_B$, (b) comes from letting $\alpha_A = \alpha_B = \alpha$. In (c), $\mathbf{G}_{u,t-1}$ is the desired ideal global gradient matrix, $\mathbf{J}_{u,t-1}$ is the global gradient error matrix caused by LoRA dropout, and can be written as $\mathbf{J}_{u,t-1} = \mathbf{G}_{u,t-1} - \hat{\mathbf{G}}_{u,t-1}$, and $\hat{\mathbf{G}}_{u,t-1} = \mathbf{B}_{u,t-1} \Delta \hat{\mathbf{A}}_{u,t-1} + \Delta \hat{\mathbf{B}}_{u,t-1} \mathbf{A}_{u,t-1}$.

Lemma 3. The layer-wise LoRA dropout error $\mathbb{E}[\|\mathbf{J}_{u,t-1}\|_F^2]$ can be bounded as

$$\begin{aligned} & \mathbb{E}[\|\mathbf{J}_{u,t-1}\|_F^2] \\ & \leq 2 \sum_{k=1}^K \frac{|\mathcal{D}_k|}{|\mathcal{D}|} \mathcal{G}^2 \mathcal{H}^2 \mathcal{G}^2 n_2 \gamma_{k,t} + 2 \sum_{k=1}^K \frac{|\mathcal{D}_k|}{|\mathcal{D}|} \mathcal{G}^2 \mathcal{H}^2 \mathcal{G}^2 n_1 \gamma_{k,t} \\ & = 2(n_1 + n_2) \mathcal{H}^2 \mathcal{G}^4 \sum_{k=1}^K \frac{|\mathcal{D}_k|}{|\mathcal{D}|} \gamma_{k,t}. \quad (25) \end{aligned}$$

Proof. Please refer to Appendix B. \square

By leveraging Assumptions 1-5 and Lemma 3, we derive the expected upper bound of the optimality gap between

consecutive training rounds by elucidating how the gradient error matrix \mathbf{J}_{t-1} affects the FT procedure.

Theorem 4. Setting the learning rate as $\alpha = \frac{1}{\eta}$, we get the upper bounding loss descent by gradient norms,

$$\begin{aligned} & \mathbb{E}[\mathcal{L}(\Delta\theta_t)] - \mathcal{L}(\Delta\theta_{t-1}) \\ & \leq -\frac{\mu\rho}{\eta} + \frac{U'(n_1 + n_2)\mathcal{H}^2\mathcal{G}^4 \sum_{k=1}^K \frac{|\mathcal{D}_k|}{|\mathcal{D}|} \gamma_{k,t}}{\eta}. \end{aligned} \quad (26)$$

Proof. Please refer to Appendix C. \square

D. Convergence Analysis

In this subsection, we investigate the convergence behavior of FedLoDrop by capturing the learning error caused by the LoRA dropout. Based on (65), we have

$$\begin{aligned} & \frac{1}{2\eta} \mathbb{E} [\|\nabla \mathcal{L}(\Delta\theta_{t-1})\|_F^2] \\ & \leq \mathbb{E}[\mathcal{L}(\Delta\theta_{t-1}) - \mathcal{L}(\Delta\theta_t)] + \frac{1}{2\eta} \mathbb{E} [\|\mathbf{J}_{t-1}\|_F^2]. \end{aligned} \quad (27)$$

Next, averaging both sides across communication rounds $t = 2, 3, \dots, T+1$, and combining with Lemma 3, the average F-norm of global gradient is bounded by

$$\begin{aligned} & \frac{1}{T} \sum_{t=2}^{T+1} \mathbb{E} [\|\nabla \mathcal{L}(\Delta\theta_{t-1})\|_F^2] \leq \frac{2\eta}{T} (\mathcal{L}(\Delta\theta_1) - \mathcal{L}(\Delta\theta^*)) \\ & + \frac{1}{T} \sum_{t=2}^{T+1} 2(n_1 + n_2) U' \mathcal{H}^2 \mathcal{G}^4 \sum_{k=1}^K \frac{|\mathcal{D}_k|}{|\mathcal{D}|} \gamma_{k,t}, \end{aligned} \quad (28)$$

where $\Delta\theta_1$ and $\Delta\theta^*$ denote the initialized model and the optimal model, respectively. It can be observed that the average F-norm of global gradient matrix is bounded by two terms: the first captures the discrepancy between $\Delta\theta_1$ and $\Delta\theta^*$, while the second reflects the optimality gap introduced by LoRA dropout. As the number of communication rounds tends to infinity, the right-hand side of (28) converges to zero. Furthermore, the convergence rate decreases with an increasing dropout rate, since FedLoDrop reduces per-round communication overhead at the cost of requiring more rounds to achieve convergence.

IV. EDGE IMPLEMENTATION OF FEDLODROP

A. System Model

1) Network Model: A single-cell network implements the FedLoDrop framework, as shown in Fig. 1. The system includes one edge server with a single-antenna access point (AP) and K single-antenna edge devices that cooperatively perform FL via wireless links. Channels are frequency non-selective, static within each round but vary across rounds. Using orthogonal frequency division multiplexing (OFDM), different users are allocated distinct subcarriers to avoid intra-cell interference. Each device uses separate subcarriers for downloading and uploading. The server obtains channel state information (CSI) of channels of all devices by using effective channel estimation methods (see, e.g., [38]).

2) Latency and Energy Consumption Models: Consider an arbitrary communication round t and device k . We ignore latency and energy consumption in the sub-adapter generation and aggregation steps. The other three steps are modeled as follows:

- *Downloading Step:* Denote the latency of device k on subcarrier s to download its assigned sub-adapter as $T_{k,t,s}^{\text{com,dl}}$. If subcarrier s is not allocated to k , i.e., $z_{k,t,s} = 0$, $T_{k,t,s}^{\text{com,dl}} = 0$. Otherwise,

$$T_{k,t,s}^{\text{com,dl}} = \frac{\hat{M}_{k,t,s} Q}{R_{k,t,s}^{\text{dl}}}, \quad \forall z_{k,t,s} = 1, \quad (29)$$

where Q is the quantization bits used for one parameter, $\hat{M}_{k,t,s}$ is the number of parameters uploaded by device k on subcarrier s . $R_{k,t,s}^{\text{dl}}$ is the channel capacity, given as

$$R_{k,t,s}^{\text{dl}} = B \log_2 \left(1 + \frac{|h_{k,t,s}^{\text{dl}}|^2 P_{k,t,s}^{\text{com,dl}}}{\sigma^2} \right), \quad (30)$$

where σ^2 is the power of additive white Gaussian noise, $h_{k,t,s}^{\text{dl}}$ is the downlink channel gain, and $P_{k,t,s}^{\text{com,dl}}$ is the downlink transmit power of device k on subcarrier s , respectively. Then, the overall uploading latency of device k is decided by the slowest subcarrier:

$$T_{k,t}^{\text{com,dl}} = \max_s T_{k,t,s}^{\text{com,dl}}. \quad (31)$$

The energy consumption in this step is to receive the model, which is included in the circuit energy consumption ξ_k .

- *Local Tuning Step:* The latency of device k is given by

$$T_{k,t}^{\text{cmp}} = \frac{C_{k,t} |\mathcal{D}_k|}{f_{k,t}}, \quad (32)$$

where $f_{k,t}$ (in cycle/s) is the CPU/GPU frequency of device k , $C_{k,t}$ is the number of processor operations to update the subnet using one data sample. Then, following [39], the energy consumption is given by

$$E_{k,t}^{\text{cmp}} = \Omega_k T_{k,t}^{\text{cmp}} (f_{k,t})^3, \quad (33)$$

where Ω_k is a constant characterizing the local computation performance of the processor on device k .

- *Uploading Step:* Denote the latency of device k on subcarrier s to upload its assigned sub-adapter as $T_{k,t,s}^{\text{com,ul}}$. If subcarrier s is not allocated to k , i.e., $z_{k,t,s} = 0$, $T_{k,t,s}^{\text{com,ul}} = 0$. Otherwise,

$$T_{k,t,s}^{\text{com,ul}} = \frac{\hat{M}_{k,t,s} Q}{R_{k,t,s}^{\text{ul}}}, \quad \forall z_{k,t,s} = 1, \quad (34)$$

where $R_{k,t,s}^{\text{ul}}$ is the channel capacity, given by

$$R_{k,t,s}^{\text{ul}} = B \log_2 \left(1 + \frac{|h_{k,t,s}^{\text{ul}}|^2 P_{k,t,s}^{\text{com,ul}}}{\sigma^2} \right). \quad (35)$$

In (35), $h_{k,t,s}^{\text{ul}}$ is the uplink channel gain, and other notations follow that in (30). Based on (35), the uplink transmit power is derived as

$$P_{k,t,s}^{\text{com,ul}} = \left(2^{\frac{R_{k,t,s}^{\text{ul}}}{B}} - 1 \right) \frac{\sigma^2}{|h_{k,t,s}^{\text{ul}}|^2}. \quad (36)$$

Then, the overall uploading latency of device k is decided by the slowest subcarrier:

$$T_{k,t}^{\text{com,ul}} = \max_s T_{k,t,s}^{\text{com,ul}}. \quad (37)$$

If subcarrier s is not allocated to k , i.e., $z_{k,t,s} = 0$, $E_{k,t,s}^{\text{com,ul}} = 0$. Otherwise, $E_{k,t,s}^{\text{com,ul}} = z_{k,t,s} P_{k,t,s}^{\text{com,ul}} T_{k,t,s}^{\text{com,ul}}$. The total uploading energy consumption of device k is the sum of uploading energy consumption over all subcarriers, given by

$$E_{k,t}^{\text{com,ul}} = \sum_{s=1}^S E_{k,t,s}^{\text{com,ul}}. \quad (38)$$

In summary, the overall latency of device k in this round is derived as

$$T_{k,t} = T_{k,t}^{\text{com,dl}} + T_{k,t}^{\text{cmp}} + T_{k,t}^{\text{com,ul}}, \quad \forall k, \quad (39)$$

where $T_{k,t}^{\text{com,dl}}$ is the downlink communication latency defined in (31), $T_{k,t}^{\text{cmp}}$ is the computation latency defined in (32), and $T_{k,t}^{\text{com,ul}}$ is the uplink communication latency defined in (37).

The total energy consumption of device k in this round is

$$E_{k,t} = E_{k,t}^{\text{com,ul}} + E_{k,t}^{\text{cmp}} + \xi_k, \quad \forall k, \quad (40)$$

where $E_{k,t}^{\text{cmp}}$ is the computation energy consumption in (33), $E_{k,t}^{\text{com,ul}}$ is the communication energy consumption in (38), and ξ_k is the circuit energy consumption for global model reception.

B. Problem Formulation

Based on the error bound provided in (23), this subsection formulates an optimization problem to jointly design the adaptive dropout rate and resource allocation, aiming to minimize this bound. Since probability δ and other parameters, i.e., C and η are constants, minimizing the right side of (23) is equivalent to

$$\begin{aligned} \min_{\{\gamma_{k,t}, z_{k,t,s}, \hat{M}_{k,t,s}\}} \quad & \frac{U'(n_1 + n_2) \mathcal{H}^2 \mathcal{G}^4 \sum_{k=1}^K \frac{|\mathcal{D}_k|}{|\mathcal{D}|} \gamma_{k,t}}{\eta} \\ & + \sqrt{\frac{\sum_{k=1}^K \frac{12C\eta^2}{\Lambda_{k,t,\min} + 2\lambda_t(2\gamma_{k,t} - \gamma_{k,t}^2)}}{|\mathcal{D}| \delta}}. \end{aligned} \quad (41)$$

Due to the limited network resources, there are several constraints on the latency, energy consumption, subcarrier allocation, and LoRA dropout rate in each round t , as elaborated below.

1) *Per-Round Latency Constraint*: The latency of each device should not exceed the maximum permitted latency T_0 to complete this round. Based on the devices' latency $\{T_{k,t}\}$ derived in (39), the latency constraint is given by

$$T_{k,t}^{\text{com,dl}} + T_{k,t}^{\text{cmp}} + T_{k,t}^{\text{com,ul}} \leq T_0, \quad \forall k. \quad (42)$$

By substituting $T_{k,t}^{\text{com,dl}}$ given in (31), $T_{k,t}^{\text{cmp}}$ given in (32), and $T_{k,t}^{\text{com,ul}}$ given in (37) into the latency constraint, we have

$$\mathcal{C}_1 : \max_s T_{k,t,s}^{\text{com,dl}} + T_{k,t}^{\text{cmp}} + \max_s T_{k,t,s}^{\text{com,ul}} \leq T_0, \quad \forall z_{k,t,s} = 1. \quad (43)$$

2) *Energy Consumption Constraint*: The total energy consumption of each device should be no larger than its energy budget $E_{k,0}$. Based on the energy consumption $\{E_{k,t}\}$ of devices given in (40), the energy consumption constraint is given by

$$\mathcal{C}_2 : E_{k,t}^{\text{com,ul}} + E_{k,t}^{\text{cmp}} + \xi_k \leq E_{k,0}, \quad \forall k, \quad (44)$$

where $E_{k,t}^{\text{cmp}}$ is defined in (33) and $E_{k,t}^{\text{com,ul}}$ is defined in (38).

3) *Subcarrier Assignment Constraint*: Each subcarrier can be allocated to one worker:

$$\mathcal{C}_3 : \begin{cases} z_{k,t,s} \in \{0, 1\}, \quad \forall k, \\ \sum_{k=1}^K z_{k,t,s} = 1. \end{cases} \quad (45)$$

where $\sum_{k=1}^K z_{k,t,s} = 1$ represents that the subcarrier s is allocated to device k .

4) *Parameter Constraint*: For each device, the total uploaded number of parameters on all subcarriers should be no smaller than its allocated subnet size:

$$\mathcal{C}_4 : \sum_{s=1}^S z_{k,t,s} \hat{M}_{k,t,s} \geq \hat{M}_{k,t}, \quad \forall k, \quad (46)$$

where $\hat{M}_{k,t} = (1 - \gamma_{k,t})M$.

5) *Dropout Rate Constraint*: Based on the definition, the dropout rate of each device in each communication round should be limited between 0 and 1, namely,

$$\mathcal{C}_5 : 0 \leq \gamma_{k,t} < 1, \quad \forall k. \quad (47)$$

Under the constraints above, the optimization problem is formulated as (48). This is a mixed-integer non-linear problem (MINLP) and thus NP-hard. In the sequel, an arbitrary round is considered and the notation t is omitted for simplicity.

V. OPTIMIZED FEDLoDROP IMPLEMENTATION

This section first presents an algorithm based on the B&B framework to jointly optimize \mathcal{P}_1 , which is a well-established approach for handling mixed binary-continuous optimization problems. To reduce the complexity, a P-SCA-based algorithm is then proposed. In the context of the OFDM systems considered in this work, the problem is further complicated by the binary subcarrier allocation among devices, along with the associated inter-subcarrier parameter allocation for each device. The resource allocation is dynamically adjusted during training, making it adaptive to changing conditions and highly practical for real-world environments. To perform this optimization, the system requires the CSI, data resource profile, and computational capacity of the devices.

A. An Equivalent Problem Formulation

To handle the integer variables, $\hat{M}_{k,s}$ are relaxed to be continuous for computational simplicity. These values are rounded to integers for implementation, with negligible loss due to the typically large magnitudes [38]. For the binary variables $z_{k,s}$, the B&B-based algorithm is employed. The core idea of B&B is to iteratively partition the feasible region and prune suboptimal subspaces through bound comparisons. Initially, the root node (i.e., the original problem) is relaxed

$$\mathcal{P}_1 : \min_{\substack{\{\gamma_{k,t}, z_{k,t,s}, \hat{M}_{k,t,s}\} \\ k \in \mathcal{K}}} \frac{U'(n_1 + n_2) \mathcal{H}^2 \mathcal{G}^4 \sum_{k=1}^K \frac{|\mathcal{D}_k|}{|\mathcal{D}|} \gamma_{k,t}}{\eta} + \sqrt{\frac{\sum_{k=1}^K \frac{12C\eta^2}{\Lambda_{k,t,\min} + 2\lambda_t(2\gamma_{k,t} - \gamma_{k,t}^2)}}{|\mathcal{D}|\delta}}, \quad (48)$$

s.t. $\mathcal{C}_1 \sim \mathcal{C}_5.$

by ignoring integrality constraints, in order to compute a bounding value. To the end, the following variables are used to transform \mathcal{P}_1 into a convex problem.

$$\begin{cases} \tilde{\gamma}_k = 1 - \gamma_k, \\ \tilde{M}_{k,s} = z_{k,s} \hat{M}_{k,s}. \end{cases} \quad (49)$$

Thus, for a given $z_{k,s}$, the primal problem of \mathcal{P}_1 can be written as

$$\mathcal{P}_2 : \min_{\substack{\{\tilde{\gamma}_k\}, \{\tilde{M}_{k,s}\}, \\ \{T_k^{\text{com,ul}}\}, \{T_k^{\text{com,dl}}\}}} \frac{I}{\eta} \sum_{k=1}^K \frac{|\mathcal{D}_k|}{|\mathcal{D}|} (1 - \tilde{\gamma}_k) + \frac{V\eta}{\sqrt{|\mathcal{D}|}} \sqrt{\sum_{k=1}^K \frac{1}{-\tilde{\gamma}_k^2 + a_k}},$$

s.t. $T_k^{\text{com,dl}} + \frac{C_k |\mathcal{D}_k|}{f_k} + T_k^{\text{com,ul}} \leq T_0,$

$$\sum_{s=1}^S \frac{\tilde{M}_{k,s} \left(2^{\frac{R_{k,s}^{\text{ul}}}{B}} - 1 \right) \sigma^2 Q}{|h_{k,s}^{\text{ul}}|^2 R_{k,s}^{\text{ul}}} + C_k |\mathcal{D}_k| \Omega_k f_k^2 + \xi_k \leq E_{k,0},$$

$$\sum_{s=1}^S \tilde{M}_{k,s} \geq \tilde{\gamma}_k M, \quad \forall k,$$

$$0 \leq \tilde{\gamma}_k < 1, \quad \forall k,$$

$$T_k^{\text{com,dl}} \geq \frac{\tilde{M}_{k,s} Q}{R_{k,s}^{\text{dl}}}, \quad \forall (k, s),$$

$$T_k^{\text{com,ul}} \geq \frac{\tilde{M}_{k,s} Q}{R_{k,s}^{\text{ul}}}, \quad \forall (k, s),$$

where $I = U'(n_1 + n_2) \mathcal{H}^2 \mathcal{G}^4$, $V = \sqrt{\frac{6C}{\delta\lambda}}$, and $a_k = \frac{2\lambda + \Lambda_{k,\min}}{2\lambda}$.

Lemma 4. Problem \mathcal{P}_2 is convex.

Proof. Please refer to Appendix D. □

B. Global Optimal Solution

As sub-problem \mathcal{P}_2 is convex, its optimal solution is obtained by the primal-dual method, which is summarized in Algorithm 2.

Remark 3. Computational Complexity Analysis: In our B&B-based method, the problem is solved iteratively. At each iteration, the primal problem, which has a complexity of $\mathcal{O}(K^2 S)$, is solved using the primal-dual method. Let I_{iter} be the number of iterations for the master problem. Thus, the total complexity is $\mathcal{O}(I_{\text{iter}} \cdot K^2 S)$, reaching up to $\mathcal{O}(2^{KS} \cdot K^2 S)$ in the worst case.

Algorithm 2: B&B-based Primal-dual Algorithm

- Input:** $\{R_k^{\text{dl}}\}, \{R_k^{\text{ul}}\}, \{P_k^{\text{com,ul}}\}, \{f_k\}, T_0, \{E_{k,0}\}$.
- 1 Initialize** $\{\zeta_s^{(0)}\}, \{\iota_k^{(0)}\}, \{\chi_k^{(0)}\}, \{\kappa_k^{(0)}\}, \{\phi_k^{(0)}\}, \{\psi_k^{(0)}\}$, the step sizes $\{\eta_{\zeta s}\}, \{\eta_{\iota k}\}, \{\eta_{\chi k}\}, \{\eta_{\kappa k}\}, \{\eta_{\phi k}\}, \{\eta_{\psi k}\}$, and $i = 0$.
- 2 Loop.**
- 3 Update the multipliers as
- $$\zeta_s^{(i+1)} = \max \left\{ \zeta_s^{(i)} + \eta_{\zeta s} \frac{\partial \mathcal{L}_{\text{P2}}}{\partial \zeta_s}, 0 \right\},$$
- $$\iota_k^{(i+1)} = \max \left\{ \iota_k^{(i)} + \eta_{\iota k} \frac{\partial \mathcal{L}_{\text{P2}}}{\partial \iota_k}, 0 \right\}, \forall k,$$
- $$\chi_k^{(i+1)} = \max \left\{ \chi_k^{(i)} + \eta_{\chi k} \frac{\partial \mathcal{L}_{\text{P2}}}{\partial \chi_k}, 0 \right\}, \forall k,$$
- 4 Calculate $\{\tilde{\gamma}_k\}$ and $\{\tilde{M}_{k,s}\}$.
- 5 Get $\{\gamma_k\}$ and $\{\hat{M}_{k,s}\}$ using (49).
- 6 $i = i + 1$.
- 7 Until Convergence.**
- Output:** $\{\gamma_k\}$ and $\{\hat{M}_{k,s}\}$.
-

C. Low-complexity suboptimal solution

Although the proposed B&B-based algorithm obtains the globally optimal solution, it may incur high computational complexity due to the iterative partitioning and search for the best-known feasible solution [40], [41]. To address this limitation, a low-complexity P-SCA-based algorithm is proposed as an alternative, aiming to strike a balance between computational efficiency and system performance.

Specifically, the non-convex constraint (C3) is converted to an equivalent form with continuous variables as follows:

$$\mathcal{C}_3 \rightarrow \begin{cases} \mathcal{C}_6 : z_{k,s} (1 - z_{k,s}) \leq 0, \\ \mathcal{C}_7 : 0 \leq z_{k,s} \leq 1. \end{cases} \quad (50)$$

By applying the penalty method, objective function of \mathcal{P}_2 is transformed to $\frac{I}{\eta} \sum_{k=1}^K \frac{|\mathcal{D}_k|}{|\mathcal{D}|} (1 - \tilde{\gamma}_k) + \frac{V\eta}{\sqrt{|\mathcal{D}|}} \sqrt{\sum_{k=1}^K \frac{1}{-\tilde{\gamma}_k^2 + a_k}} + \tau \sum_{k=1}^K \sum_{s=1}^S (z_{k,s} - z_{k,s}^2)$. Approximating the objective function by using the first-order Taylor expansion, $z_{k,s} - z_{k,s}^2$ is rewritten as a difference-of-convex (DC) function shown as $z_{k,s} - z_{k,s}^2 = \Psi_1(z_{k,s}) - \Psi_2(z_{k,s})$, where $\Psi_1(z_{k,s}) = z_{k,s}$, $\Psi_2(z_{k,s}) = z_{k,s}^2$. Thus, the convex lower bound of $\Psi_2(z_{k,s})$ can be obtained by the first-order Taylor expansion, i.e.,

$$\bar{\Psi}_2(z_{k,s}) = \Psi_2(\bar{z}_{k,s}) + \nabla \Psi_2(\bar{z}_{k,s})(z_{k,s} - \bar{z}_{k,s}) = 2\bar{z}_{k,s} z_{k,s} - (\bar{z}_{k,s})^2, \quad (51)$$

where $\bar{z}_{k,s}$ is represents a feasible solution to Problem \mathcal{P}_2 . With $\bar{\Psi}_2(z_{k,s})$, $z_{k,s} - z_{k,s}^2$ is approximated by its convex upper

TABLE I
GLUE BENCHMARK

Method	CoLa (Mcc)	RTE	MRPC	SST-2	QNLI	STS-B (Corr)	Avg
FedIT in [20]	62.08	77.26	90.44	95.99	94.86	91.54	85.36
FedLoDrop (0.2)	63.56	78.70	89.46	96.67	94.95	91.34	85.78
FedLoDrop (0.3)	62.84	81.6	88.48	96.56	95.17	90.84	85.92
FFA in [23]	58.32	70.76	87.49	95.59	93.85	90.24	82.71
FFA with Bernoulli Dropout (0.2)	62.37	74.73	83.33	95.76	94.55	89.12	83.31
FFA with Bernoulli Dropout (0.3)	61.83	69.31	78.18	96.22	94.29	88.84	81.45
FedIT with Gaussian Dropout (0.2)	62.08	77.98	90.20	96.22	94.25	91.72	85.41
FedIT with Gaussian Dropout (0.3)	61.82	77.98	89.22	95.41	93.85	91.47	84.96

bound denoted as $z_{k,s} - z_{k,s}^2 \leq \Psi_1(z_{k,s}) - \bar{\Psi}_2(z_{k,s})$. An upper bound of the problem can be found by solving

$$\mathcal{P}_3 \min_{\{\tilde{\gamma}_k\}, \{\tilde{M}_{k,s}\}, \{z_{k,s}\}, \{T_k^{\text{com}, \text{ul}}\}, \{T_k^{\text{com}, \text{dl}}\}} \frac{I}{\eta} \sum_{k=1}^K \frac{|\mathcal{D}_k|}{|\mathcal{D}|} (1 - \tilde{\gamma}_k) + \frac{V\eta}{\sqrt{|\mathcal{D}|}} \sqrt{\sum_{k=1}^K \frac{1}{-\tilde{\gamma}_k^2 + a_k} + \tau \sum_{k=1}^K \sum_{s=1}^S (1 - 2\bar{z}_{k,s}) z_{k,s} + (\bar{z}_{k,s})^2}$$

Note that problem \mathcal{P}_3 is convex and can be solved by using the primal-dual method as well.

Remark 4. Computational Complexity Analysis: solving problem \mathcal{P}_3 is with the complexity order of $\mathcal{O}(I'_{\text{iter}} \cdot K^2 S)$, where I'_{iter} represents the iteration numbers.

VI. SIMULATION RESULTS

We evaluate the superiority of the proposed FedLoDrop framework and compare it with other baseline methods on two major NLP tasks: natural language understanding (NLU) and question answering (QA). We first fine-tune two LLMs including RoBERTa large (355M) and LLaMA (7B) on two benchmarks including GLUE and MMLU. Following the configurations in the original LoRA paper [8], the LoRA modules are applied to the self-attention layers. For RoBERTa large, LoRA rank is set as 4 in a three-client cross-silo federated setting, and $r = 16$ with 10 devices for LLaMA in [23], [42]. The local batch size, epoch and learning rate are set to be 64, 1, and 3e-4, respectively. The AdamW optimizer is adopted during the training. The downlink channel gains of devices are assumed to be Rayleigh fading. The path loss is 10^{-3} . For data distribution among clients, a common method of randomly sampling non-IID data for each client is employed, as implemented in [20], [43]. Experiments are performed using 4 NVIDIA RTX 4090 (24 GB each) GPUs.

A. Effects of Dropout Rate

Fixed-rate experiments are conducted for ablation and sensitivity analysis, which establish a baseline performance landscape to compare how different levels of regularization (dropout rates) affect final model accuracy and convergence. Table I presents the results of RoBERTa-large on the GLUE benchmark. It can be observed that models incorporating the

dropout method generally achieve superior performance, suggesting that the proposed FedLoDrop framework helps LoRA-based models control overfitting and enhance generalization on downstream tasks. The framework is also applicable to FFA [23]. In contrast to FedLoDrop, when the dropout rate is set to 0.3, the average score begins to decline. This is attributed to fewer parameters being updated under this setting, which limits model adaptability and consequently reduces performance.

To visualize the trend, we plot the effects of dropout rate on the performance, as shown in Fig. 2. For LLaMA, we selected 1444 samples from the dataset for a quick and comprehensive evaluation, noted as Sampled. For MMLU, among 57 disciplines, Humanities, Stem, and Average are plotted. In both figures, as the dropout rate increases, the accuracy first improves and then drops. This aligns with the theoretical derivation that a proper dropout rate would help balance the adaptation function's empirical risk minimization and complexity. A small dropout rate might fail to introduce sufficient sparsity and lead to overfitting, while an excessively large dropout rate would result in too few trainable parameters, making the adapter lose its expressive power. This contrast underscores the necessity of finding an optimal, and potentially dynamic, dropout strategy.

To evaluate sensitivity to the dropout distribution, we compare Bernoulli and Gaussian dropout. Gaussian dropout multiplies activations by a continuous random variable drawn from $\mathcal{N}(1, \sigma_{\text{gaus}}^2)$ instead of setting them to zero. The results on RoBERTa-large and LLaMA models are presented in Table I and Fig. 2(b), respectively. The comparable performance of both methods demonstrates the robustness to the specific implementation of dropout. Bernoulli dropout provides more stable results across a wider range of rates, while Gaussian dropout yields slightly better performance at lower rates (e.g., 0.2 for RoBERTa-large, 0.1 for LLaMA), likely because its continuous noise injection prevents the complete silencing of neurons. In contrast, higher dropout rates lead to exploding variance, potentially destabilizing the training process.

B. Effects of Network Resources

To verify the superiority of the proposed two schemes, the following benchmark schemes are compared under different network resources. 1) *Scheme Without Dropout*: Sufficient

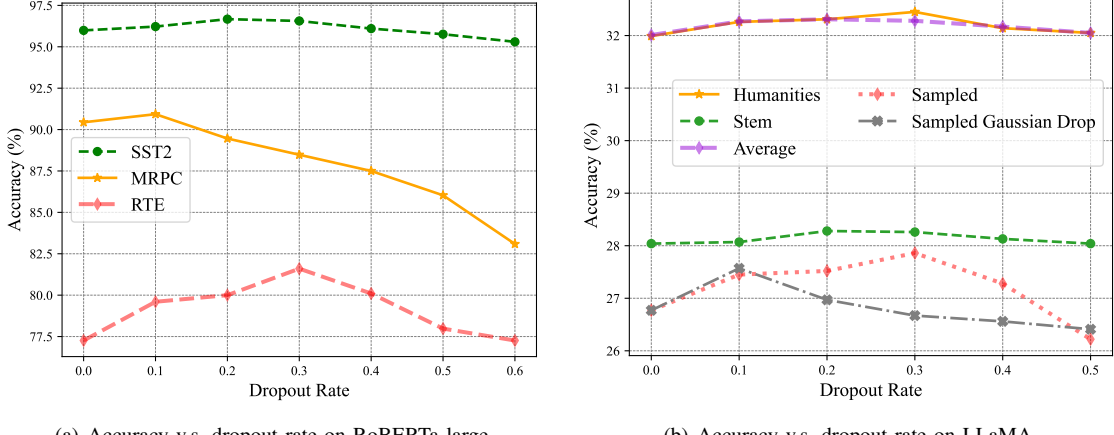


Fig. 2. Effects of dropout rate on the performance.

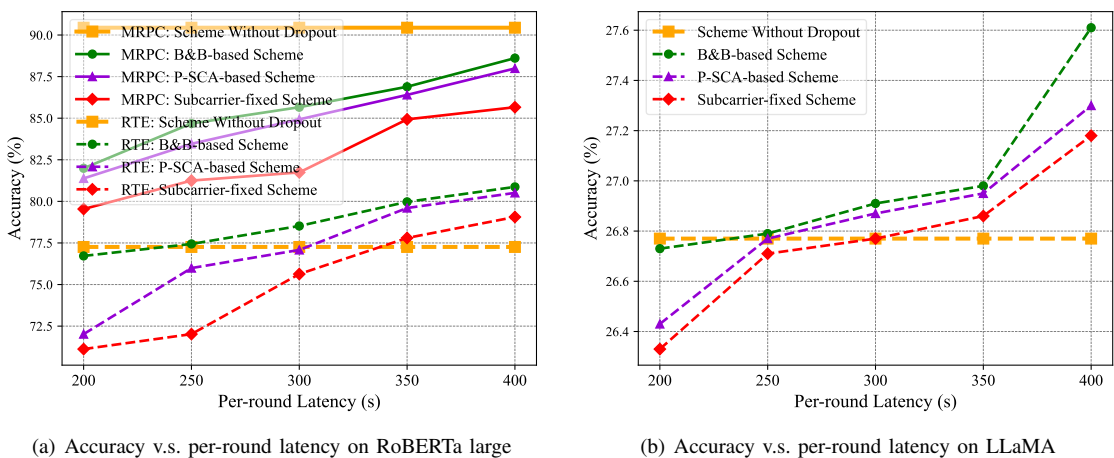


Fig. 3. Effects of per-round latency on the performance.

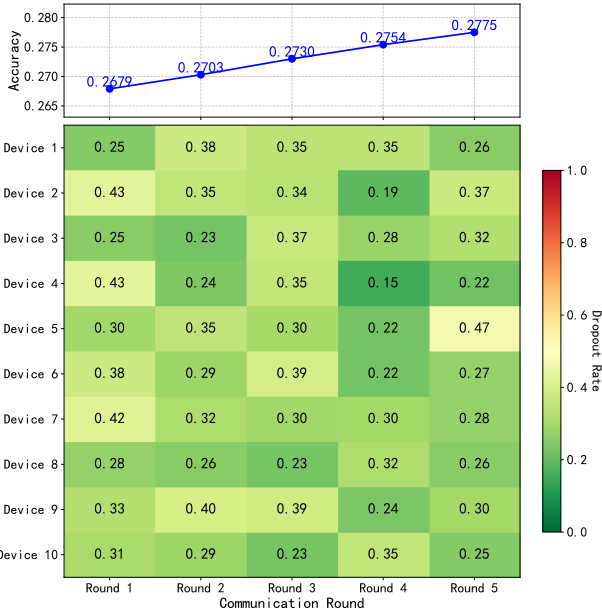


Fig. 4. The evolution of the optimized dropout rates under different rounds.
 resource is allocated and dropout is not considered, which is an ideal benchmark used to compare with the proposed schemes. 2) *Subcarrier-fixed Scheme*: Subcarrier is fixed, and

then optimize the remaining variables the same as the proposed ones. Fig. 3 illustrates the model accuracy v.s. different per-round latencies. It can be observed that, under a given per-round latency threshold, both the proposed B&B-based and the P-SCA-based algorithms outperform the subcarrier-fixed scheme when the constraint is satisfied. The P-SCA-based algorithm is capable of obtaining a suboptimal solution with performance close to that of the optimal method. Furthermore, as the allowable per-round training delay increases, the model performance tends to improve. This is attributed to a looser constraint allowing for a lower dropout rate, which effectively reduces the noise introduced during training and thereby enhances overall performance.

The evolution of the optimized dropout rates for a subset of clients over the training rounds can be shown in Fig. 4. Fig. 4 is plotted under the per-round latency of 400s. This visualization clearly shows how our algorithm dynamically adjusts the dropout rate (regularization strength) per device based on their real-time CSI and state. Simultaneously, the testing accuracy improves as the number of communication rounds increases, indicating effective learning despite adaptive parameter reduction.

In addition to reporting the final accuracy to evaluate generalization performance, we present the global testing accuracy

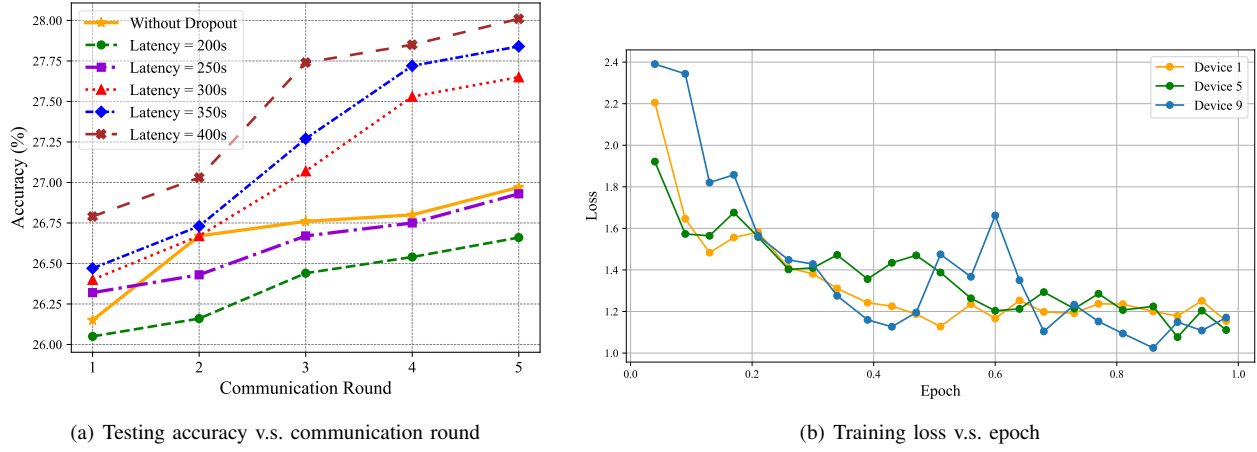


Fig. 5. Convergence performance.

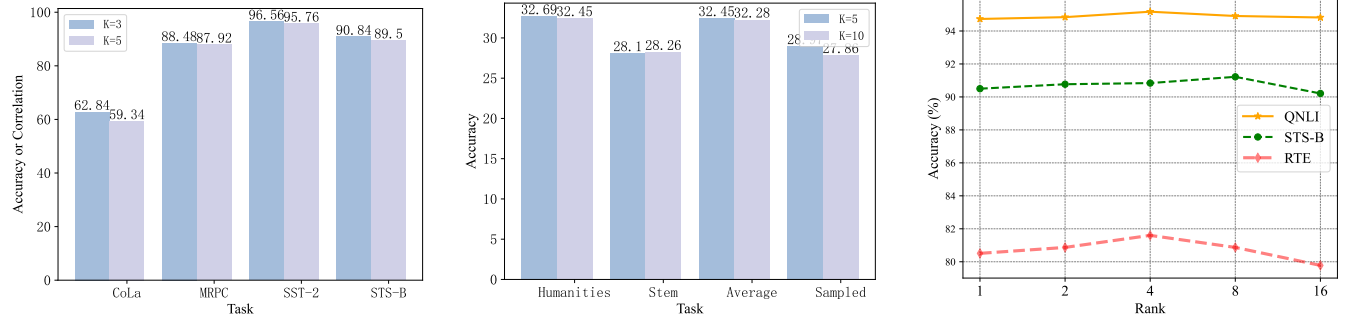


Fig. 6. Effects of parameters on the performance.

v.s. communication round and the device training loss v.s. epoch to illustrate the convergence behavior, as shown in Fig. 5(a) and Fig. 5(b), respectively. For clarity, we plot the training loss of three representative devices. The standard federated LoRA scheme is denoted by 'Without Dropout'. It can be observed that the convergence rate improves under a looser per-round latency constraint, which aligns with the theoretical analysis in Section III-D.

C. Effects of Resource Utilization Efficiency

1) *Per-round Latency*: As shown in Fig. 3(a) and Fig. 3(b), given a fixed target accuracy, the proposed B&B-based and P-SCA-based algorithms achieve the same performance with shorter per-round latency compared to the subcarrier-fixed scheme. This improvement is attributed to the reduced number of transmitted parameters. Notably, when targeting a higher accuracy (e.g., 27.2% on LLaMA), the subcarrier-fixed scheme and the scheme without dropout fail to achieve the desired performance (27.2% testing accuracy), highlighting the limitations of fixed resource allocation under stringent latency and accuracy requirements.

2) *Communication Overhead*: To quantify communication overhead, we compare the communicated parameters of the full model FT, FedIT, and FedLoDrop across 5 communication

rounds. The results show that FedLoDrop achieves the lowest communication cost, transmitting only 7.6% of the parameters required by full FT, while FedIT transmits 9.5%. By transmitting only a subset of the model parameters, FedLoDrop significantly reduces the volume of data exchanged per round compared to full FT approaches.

D. Effects of Parameters and Models

Fig. 6 presents the effects of parameters on the performance. From Fig. 6(a) and Fig. 6(b), one can see that in both models, a larger number of devices generally results in a lower testing accuracy due to the difficulty in adapting to one global model. As shown in 6(c), extremely increasing the rank results in performance deterioration, likely due to overfitting. This highlights that performance does not always improve with more trainable parameters across different tasks.

As a final stress test for FedLoDrop, we scale up to Yi-34B. Due to the high training cost, we only report the results for given dropout rates. The LoRA rank is set as 16, with the learning rate of $3e-4$. Experiments are performed on 2 NVIDIA A100 (40 GB each) GPUs. As shown in Table II, FedLoDrop with 0.2 dropout rate achieves the best performance, consistent with the findings in Section VI-A. For brevity and due to space constraints, we omit the full results.

VII. CONCLUSION

In this paper, we propose a new framework, called FedLoDrop, which effectively incorporates a parameter-efficient

TABLE II
ACCURACY V.S. DROPOUT RATE ON YI-34B.

Dropout Rate	0	0.1	0.2	0.3
Accuracy	43.04	43.35	43.39	42.54

finetuning technique, known as LoRA, to facilitate local training. This method reduces computational and communication overheads for local edge devices that have limited resources. We analytically demonstrate the trade-off between underfitting and overfitting by deriving mechanisms that elucidate these dynamics. The application of dropout alleviates the imbalanced update of the parameter matrix and mitigates parameter overfitting in LoRA. Specifically, PHS-based analysis reveals that increasing the dropout rate narrows the gap between empirical and generalization errors but also increases empirical error. Based on this insight, we propose two schemes, B&B-based and P-SCA-based algorithms to minimize the generalization error bound by jointly optimizing the dropout rate and network resource allocation, thereby enhancing the learning performance. Frameworks for collaborative federated sensing and communication systems will be left for future directions. Besides, in future work, the proposed FedLoDrop can be extended to multi-modal large language models (MLLMs) to dynamically adjust local dropout strategies based on modality importance or client-specific resource constraints.

APPENDIX A PROOF OF THEOREM 1

A. Proof of Theorem 2

Lemma 5. Consider the learning algorithm M optimizing the following loss function:

$$\min_{\theta_{k,t}} \ell_{k,\lambda_t}(\theta_{k,t}) = \min_{\theta_{k,t}} \ell_{k,t}(\theta_{k,t}) + \lambda_t \|\theta_{k,t} - \theta_0\|_2^2. \quad (52)$$

If the requirements in Definition 1 are met, then it has PHS $\beta = \frac{2\eta^2}{(\Lambda_{k,t,\min} + 2\lambda_t)|\mathcal{D}_k|}$, which is

$$\begin{aligned} \mathbb{E}_{\mathcal{D}_k, j \sim U(n)} \left| \ell_{k,\lambda_t} \left(\theta_{\ell_{k,\lambda_t}}(\mathcal{D}_k^j), \mathbf{x}_j \right) - \ell_{k,\lambda_t} \left(\theta_{\ell_{k,\lambda}}(\mathcal{D}_k), \mathbf{x}_j \right) \right| \\ \leq \frac{2\eta^2}{(\Lambda_{k,t,\min} + 2\lambda_t)|\mathcal{D}_k|}. \end{aligned} \quad (53)$$

Proof. Denote $\theta_{\ell_{k,\lambda_t}}(\mathcal{D}_k)$ as $\hat{\theta}_{k,t}$, and $\Delta\hat{\theta}_{k,t} = \hat{\theta}_{k,t} - \theta$. Consider the second-order Taylor expansion of ℓ_{k,λ_t} at local optimal $\hat{\theta}_{k,t}$, $\nabla_{\ell_{k,\lambda_t}}(\hat{\theta}_{k,t}) = 0$. Thus, for $\forall v$ close to $\hat{\theta}_{k,t}$,

$$\ell_{k,\lambda_t}(v) = \ell_{k,\lambda_t}(\hat{\theta}_{k,t}) + \frac{1}{2}(v - \hat{\theta}_{k,t})^\top \nabla^2 \ell_{k,\lambda_t}(\hat{\theta}_{k,t})(v - \hat{\theta}_{k,t}). \quad (54)$$

Then, expand $\nabla^2 \ell_{k,\lambda_t}(\hat{\theta}_k)$ in (54),

$$\begin{aligned} \nabla^2 \ell_{k,\lambda_t}(\hat{\theta}_k) &= \nabla^2_{\theta_{k,t}} (\ell_{k,t}(\hat{\theta}_{k,t}) + \lambda_t \|\hat{\theta}_{k,t} - \theta_0\|_2^2) \\ &= \nabla^2 \ell_{k,t}(\hat{\theta}_{k,t}) + 2\lambda_t I = U_{k,t} \text{diag}(\Lambda_{k,t}) U_{k,t}^{-1} + 2\lambda_t I \\ &= U_{k,t} (\text{diag}(\Lambda_{k,t}) + 2\lambda_t I) U_{k,t}^{-1} \\ &= U_{k,t} \text{diag}(\sqrt{\Lambda_{k,t,1} + 2\lambda_t}, \dots, \sqrt{\Lambda_{k,t,d} + 2\lambda_t}) U_{k,t}^{-1} \\ &\quad \text{diag}(\sqrt{\Lambda_{k,t,1} + 2\lambda_t}, \dots, \sqrt{\Lambda_{k,t,d} + 2\lambda_t}) U_{k,t}^{-1}. \end{aligned} \quad (55)$$

Take this back to (54),

$$\begin{aligned} \ell_{k,\lambda_t}(v) - \ell_{k,\lambda_t}(\hat{\theta}_{k,t}) \\ = \frac{1}{2} \|(U_{k,t} \text{diag}(\sqrt{\Lambda_{k,t,1} + 2\lambda_t}, \dots, \sqrt{\Lambda_{k,t,d} + 2\lambda_t}) U_{k,t}^{-1}) \\ (v - \hat{\theta}_{k,t})\|_2^2 \geq \frac{1}{2} (\Lambda_{k,t,\min} + 2\lambda_t) \|v - \hat{\theta}_{k,t}\|_2^2. \end{aligned} \quad (56)$$

According to the definition of $\ell_{k,\lambda_t}(\hat{\theta}_{k,t})$, for $\forall u, v$ close to $\hat{\theta}_{k,t}$, (57) is got. Take $u = \theta_{\ell_{k,\lambda_t}}(\mathcal{D}_k^j)$ and $v = \theta_{\ell_{k,\lambda_t}}(\mathcal{D}_k)$,

$$\begin{aligned} \ell_{k,\lambda_t}(\theta_{\ell_{k,\lambda_t}}(\mathcal{D}_k^j)) - \ell_{k,\lambda_t}(\theta_{\ell_{k,\lambda_t}}(\mathcal{D}_k)) \\ \leq \frac{\ell_{k,\lambda_t}(\theta_{\ell_{k,\lambda_t}}(\mathcal{D}_k^j), \mathbf{x}_j) - \ell_{k,\lambda_t}(\theta_{\ell_{k,\lambda_t}}(\mathcal{D}_k), \mathbf{x}_j)}{|\mathcal{D}_k|}, \end{aligned} \quad (58)$$

take (56) into (58),

$$\begin{aligned} \frac{1}{2} (\Lambda_{k,t,\min} + 2\lambda_t) \|\theta_{\ell_{k,\lambda_t}}(\mathcal{D}_k^j) - \theta_{\ell_{k,\lambda_t}}(\mathcal{D}_k)\|_2^2 \\ \leq \frac{\ell_{k,\lambda_t}(\theta_{\ell_{k,\lambda_t}}(\mathcal{D}_k^j), \mathbf{x}_j) - \ell_{k,\lambda_t}(\theta_{\ell_{k,\lambda_t}}(\mathcal{D}_k), \mathbf{x}_j)}{|\mathcal{D}_k|}. \end{aligned} \quad (59)$$

Because the loss function is η -Lipschitz, thus,

$$\begin{aligned} \left| \ell_{k,\lambda_t}(\theta_{\ell_{k,\lambda_t}}(\mathcal{D}_k^j), \mathbf{x}_j) - \ell_{k,\lambda_t}(\theta_{\ell_{k,\lambda_t}}(\mathcal{D}_k), \mathbf{x}_j) \right| \\ \leq \frac{\eta \|\theta_{\ell_{k,\lambda_t}}(\mathcal{D}_k^j) - \theta_{\ell_{k,\lambda_t}}(\mathcal{D}_k)\|}{|\mathcal{D}_k|}. \end{aligned} \quad (60)$$

Take (60) into (59), and basic calculation,

$$\|\theta_{\ell_{k,\lambda_t}}(\mathcal{D}_k^j) - \theta_{\ell_{k,\lambda_t}}(\mathcal{D}_k)\| \leq \frac{2\eta}{(\Lambda_{k,\min} + 2\lambda) |\mathcal{D}_k|}. \quad (61)$$

Plug (61) into (60), and as this holds for any j and \mathcal{D}_k , the proof of Lemma 5 is finished. \square

B. PHS upper bound of FedLoDrop

Consider loss function with sparsity regularization,

$$\begin{aligned} \ell_{k,\lambda_t}(\theta_{k,t}) &= \ell_{k,t}(\theta_k) + \lambda_t \mathbb{E}_{\mathbf{d}_{k,t} \sim \text{Bern}(2\gamma_{k,t} - \gamma_{k,t}^2)} \sum_j d_{k,t,j}^2 (\theta_{k,t,j} - \theta_{0,j})^2 \\ &= \ell_{k,t}(\theta_k) + \lambda_t \sum_j (\theta_{k,t,j} - \theta_{0,j})^2 \mathbb{E}_{\mathbf{d}_{k,t,j} \sim \text{Bern}(2\gamma_{k,t} - \gamma_{k,t}^2)} d_{k,t,j}^2 \\ &= \ell_{k,t}(\theta_k) + \lambda_t \sum_j (\theta_{k,t,j} - \theta_{0,j})^2 (2\gamma_{k,t} - \gamma_{k,t}^2) \\ &= \ell_{k,t}(\theta_k) + \lambda_t (2\gamma_{k,t} - \gamma_{k,t}^2) \|\theta_{k,t} - \theta_0\|^2. \end{aligned} \quad (62)$$

Integrating the result above to Lemma 5 and substituting the regularization coefficient with $\lambda(2\gamma_{k,t} - \gamma_{k,t}^2)$ finalizes the proof.

APPENDIX B PROOF OF LEMMA 3

Denote $\hat{\mathbf{J}}_{u,k,A,t-1} = \Delta \mathbf{A}_{u,k,t-1} - \Delta \hat{\mathbf{A}}_{u,k,t-1}$, $\hat{\mathbf{J}}_{u,k,B,t-1} = \Delta \mathbf{B}_{u,k,t-1} - \Delta \hat{\mathbf{B}}_{u,k,t-1}$, thus

$$\begin{aligned}
\ell_{k,\lambda_t}(u) - \ell_{k,\lambda_t}(v) &= \left(\frac{1}{|\mathcal{D}_k|} \sum_{x_i \in \mathcal{D}_k} \ell_k(u, \mathbf{x}_i) + \lambda_t \|u - \boldsymbol{\theta}_0\|_2^2 \right) - \left(\frac{1}{|\mathcal{D}_k|} \sum_{x_i \in \mathcal{D}_k} \ell_k(v, \mathbf{x}_i) + \lambda_t \|v - \boldsymbol{\theta}_0\|_2^2 \right) \\
&= \left(1 - \frac{1}{|\mathcal{D}_k|} \right) \left(\frac{1}{|\mathcal{D}_k| - 1} \sum_{i \neq j} \ell_k(u, \mathbf{x}_i) + \lambda_t \|u - \boldsymbol{\theta}_0\|_2^2 \right) - \left(1 - \frac{1}{|\mathcal{D}_k|} \right) \left(\frac{1}{|\mathcal{D}_k| - 1} \sum_{i \neq j} \ell_k(v, \mathbf{x}_i) + \lambda_t \|v - \boldsymbol{\theta}_0\|_2^2 \right) \\
&\quad + \frac{\lambda_t(\|u - \boldsymbol{\theta}_0\|_2^2 - \|v - \boldsymbol{\theta}_0\|_2^2)}{|\mathcal{D}_k|} + \frac{\ell_k(u, \mathbf{x}_j) - \ell_k(v, \mathbf{x}_j)}{|\mathcal{D}_k|} \\
&= \left(1 - \frac{1}{|\mathcal{D}_k|} \right) \left[\left(\frac{1}{|\mathcal{D}_k| - 1} \sum_{i \neq j} \ell_k(u, \mathbf{x}_i) + \lambda_t \|u - \boldsymbol{\theta}_0\|_2^2 \right) - \left(\frac{1}{|\mathcal{D}_k| - 1} \sum_{i \neq j} \ell_k(v, \mathbf{x}_i) + \lambda_t \|v - \boldsymbol{\theta}_0\|_2^2 \right) \right] \\
&\quad + \frac{\ell_{k,\lambda_t}(u, \mathbf{x}_j) - \ell_{k,\lambda_t}(v, \mathbf{x}_j)}{|\mathcal{D}_k|}.
\end{aligned} \tag{57}$$

$$\begin{aligned}
&\mathbb{E} [\|\mathbf{J}_{u,t-1}\|_F^2] \\
&= \mathbb{E} \left[\left\| \sum_{k=1}^K \frac{|\mathcal{D}_k|}{|\mathcal{D}|} (\mathbf{G}_{u,k,t-1} - \hat{\mathbf{G}}_{u,k,t-1}) \right\|_F^2 \right] \\
&= \mathbb{E} \left[\left\| \sum_{k=1}^K \frac{|\mathcal{D}_k|}{|\mathcal{D}|} (\mathbf{B}_{u,t-1} \hat{\mathbf{J}}_{u,k,A,t-1} + \hat{\mathbf{J}}_{u,k,B,t-1} \mathbf{A}_{u,t-1}) \right\|_F^2 \right] \\
&\stackrel{(a)}{\leq} 2 \sum_{k=1}^K \frac{|\mathcal{D}_k|}{|\mathcal{D}|} \mathbb{E} [\|\mathbf{B}_{u,t-1} \hat{\mathbf{J}}_{u,k,A,t-1}\|_F^2] \\
&\quad + 2 \sum_{k=1}^K \frac{|\mathcal{D}_k|}{|\mathcal{D}|} \mathbb{E} [\|\mathbf{A}_{u,t-1} \hat{\mathbf{J}}_{u,k,B,t-1}\|_F^2],
\end{aligned} \tag{63}$$

where (a) comes from the convexity of F -norm. The Taylor expansion is adopted to approximate the weights of neural networks, i.e., $\Delta \hat{\mathbf{A}}_{u,k,t-1} = \Delta \mathbf{A}_{u,k,t-1} + O(\hat{\mathbf{A}}_{u,k,t-1} - \mathbf{A}_{u,k,t-1}) + \mathbf{H}(\mathbf{A}_{u,k,t-1})(\hat{\mathbf{A}}_{u,k,t-1} - \mathbf{A}_{u,k,t-1})$. Under Assumption 3, the last higher order on the right side can be ignored. Thus,

$$\begin{aligned}
&\mathbb{E} [\|\hat{\mathbf{J}}_{u,k,A,t-1}\|_F^2] \\
&= \mathbb{E} [\|-\mathbf{H}(\mathbf{A}_{u,k,t-1})(\hat{\mathbf{A}}_{u,k,t-1} - \mathbf{A}_{u,k,t-1})\|_F^2] \\
&\leq \mathcal{H}^2 \cdot \mathbb{E} [\|\mathbf{A}_{u,k,t-1}(\text{diag}(\mathbf{m}_{A,k,t-1}) - \mathbf{I})\|_F^2] \\
&\leq \mathcal{H}^2 \mathcal{G}^2 \mathbb{E} \left[\sum_{q=1}^{n_2} (m_{A,k,t-1,q} - 1)^2 \right] = \mathcal{H}^2 \mathcal{G}^2 n_2 \gamma_{k,t}.
\end{aligned} \tag{64}$$

Take (64) back into (63), and minor changes to $\mathbb{E} [\|\hat{\mathbf{J}}_{u,k,B,t-1}\|_F^2]$, Lemma 3 has been proven.

APPENDIX C PROOF OF THEOREM 4

According to Assumption 1, set $\alpha = \frac{1}{\eta}$, and take expectation on both sides,

$$\begin{aligned}
&\mathbb{E}[\mathcal{L}(\Delta \boldsymbol{\theta}_t)] - \mathcal{L}(\Delta \boldsymbol{\theta}_{t-1}) \\
&\leq -\frac{1}{2\eta} \|\nabla \mathcal{L}(\Delta \boldsymbol{\theta}_{t-1})\|_F^2 + \frac{1}{2\eta} \mathbb{E} [\|\mathbf{J}_{t-1}\|_F^2] \\
&\leq -\frac{\mu\rho}{\eta} + \frac{1}{2\eta} \mathbb{E} [\|\mathbf{J}_{t-1}\|_F^2].
\end{aligned} \tag{65}$$

As $\mathbf{J}_{t-1} \triangleq \{\mathbf{J}_{u,t-1}\}_{u=1}^{U'}$, it can be further written as

$$\begin{aligned}
\mathbb{E} [\|\mathbf{J}_{t-1}\|_F^2] &= \mathbb{E} \left[\left\| \begin{pmatrix} \mathbf{J}_{1,t-1} \\ \vdots \\ \mathbf{J}_{u,t-1} \\ \vdots \\ \mathbf{J}_{U',t-1} \end{pmatrix} \right\|_F^2 \right] \\
&= \sum_{u=1}^{U'} \mathbb{E} [\|\mathbf{J}_{u,t-1}\|_F^2] = U' \mathbb{E} [\|\mathbf{J}_{u,t-1}\|_F^2].
\end{aligned} \tag{66}$$

Taking this back to (65), and combining it with Lemma 3, the proof is completed.

APPENDIX D PROOF OF LEMMA 4

All the constraints and objective function can be derived by substituting the variable transformation in (49). The first term in the objective function is convex. For the second one, considering two dimensions, e.g., γ_1, γ_2 , its Hessian matrix is

$$\begin{bmatrix} o_{11} & o_{12} \\ o_{21} & o_{22} \end{bmatrix}$$

where, $o_{11} = \frac{4\gamma_1^2}{(a_1 - \tilde{\gamma}_1^2)^3 \sqrt{\frac{1}{a_1 - \tilde{\gamma}_1^2} + \frac{1}{a_2 - \tilde{\gamma}_2^2}}} - \frac{\gamma_1^2}{(a_1 - \tilde{\gamma}_1^2)^4 (\frac{1}{a_1 - \tilde{\gamma}_1^2} + \frac{1}{a_2 - \tilde{\gamma}_2^2})^{3/2}} + \frac{1}{(a_1 - \tilde{\gamma}_1^2)^2 \sqrt{\frac{1}{a_1 - \tilde{\gamma}_1^2} + \frac{1}{a_2 - \tilde{\gamma}_2^2}}}, o_{12} = o_{21} = -\frac{\gamma_1 \gamma_2}{(a_1 - \tilde{\gamma}_1^2)^2 (a_2 - \tilde{\gamma}_2^2)^2 (\frac{1}{a_1 - \tilde{\gamma}_1^2} + \frac{1}{a_2 - \tilde{\gamma}_2^2})^{3/2}}, o_{22} = \frac{4\gamma_2^2}{(a_2 - \tilde{\gamma}_2^2)^3 \sqrt{\frac{1}{a_1 - \tilde{\gamma}_1^2} + \frac{1}{a_2 - \tilde{\gamma}_2^2}}} - \frac{\gamma_2^2}{(a_2 - \tilde{\gamma}_2^2)^4 (\frac{1}{a_1 - \tilde{\gamma}_1^2} + \frac{1}{a_2 - \tilde{\gamma}_2^2})^{3/2}} + \frac{1}{(a_2 - \tilde{\gamma}_2^2)^2 \sqrt{\frac{1}{a_1 - \tilde{\gamma}_1^2} + \frac{1}{a_2 - \tilde{\gamma}_2^2}}}$, and is non-negative. The higher dimensions can be generalized with inductions and definitions. Therefore, the overall objective function is convex. Besides, all constraints are linear relations, and thus are convex. Thus, Problem \mathcal{P}_2 is convex.

REFERENCES

- [1] Y. Shen, J. Shao, X. Zhang, Z. Lin, H. Pan, D. Li, J. Zhang, and K. B. Letaief, "Large language models empowered autonomous edge AI for connected intelligence," *IEEE Commun. Mag.*, vol. 62, no. 10, pp. 140–146, 2024.
- [2] J. Du, T. Lin, C. Jiang, Q. Yang, C. F. Bader, and Z. Han, "Distributed foundation models for multi-modal learning in 6G wireless networks," *IEEE Wireless Commun.*, vol. 31, no. 3, pp. 20–30, 2024.

- [3] P. Jiang, C.-K. Wen, X. Yi, X. Li, S. Jin, and J. Zhang, “Semantic communications using foundation models: Design approaches and open issues,” *IEEE Wireless Commun.*, vol. 31, no. 3, pp. 76–84, 2024.
- [4] F. Jiang, C. Pan, L. Dong, K. Wang, M. Debbah, D. Niyato, and Z. Han, “A comprehensive survey of large AI models for future communications: Foundations, applications and challenges,” *arXiv preprint arXiv:2505.03556*, 2025.
- [5] F. Wu, J. Hu, G. Min, and S. Wang, “Adaptive rank allocation for federated parameter-efficient fine-tuning of language models,” *arXiv preprint arXiv:2501.14406*, 2025.
- [6] B. Zhu, Y. Niu, Y. Han, Y. Wu, and H. Zhang, “Prompt-aligned gradient for prompt tuning,” in *Proc. IEEE/CVF Int. Conf. Comput. Vis. (ICCV)*, 2023, pp. 15 659–15 669.
- [7] J. Bai, Z. Yan, Z. Yang, J. Yang, X. Liang, H. Guo, and Z. Li, “Knowprefix-tuning: A two-stage prefix-tuning framework for knowledge-grounded dialogue generation,” in *Proc. Euro. Conf. Mach. Learn. (ECML)*, 2023, pp. 525–542.
- [8] E. J. Hu, Y. Shen, P. Wallis, Z. Allen-Zhu, Y. Li, S. Wang, L. Wang, and W. Chen, “LoRA: Low-rank adaptation of large language models,” in *Proc. Int. Conf. Learn. Represent. (ICLR)*, 2022.
- [9] K. Kuo, A. Raje, K. Rajesh, and V. Smith, “Federated Lora with sparse communication,” *arXiv preprint arXiv:2406.05233*, 2024.
- [10] X. Qiu, T. Hao, S. Shi, X. Tan, and Y.-J. Xiong, “Chain-of-LoRA: Enhancing the instruction fine-tuning performance of low-rank adaptation on diverse instruction set,” *IEEE Signal Process Lett.*, vol. 31, pp. 875–879, 2024.
- [11] H. Wu, X. Chen, and K. Huang, “Resource management for low-latency cooperative fine-tuning of foundation models at the network edge,” *IEEE Trans. Wireless Commun.*, vol. 24, no. 6, pp. 4839–4852, 2025.
- [12] G. Qu, Q. Chen, W. Wei, Z. Lin, X. Chen, and K. Huang, “Mobile edge intelligence for large language models: A contemporary survey,” *IEEE Commun. Surv. Tutorials*, pp. 1–1, 2025.
- [13] D. Wen, S. Xie, X. Cao, Y. Cui, J. Xu, Y. Shi, and S. Cui, “Integrated sensing, communication, and computation for over-the-air federated edge learning,” *IEEE Trans. Wireless Commun.*, pp. 1–1, 2025.
- [14] W. Ni, H. Ao, H. Tian, Y. C. Eldar, and D. Niyato, “Fedsl: Federated split learning for collaborative healthcare analytics on resource-constrained wearable iomt devices,” *IEEE Internet Things J.*, vol. 11, no. 10, pp. 18 934–18 935, 2024.
- [15] X. Shang, Z. Liu, D. Gao, D. Yang, W. Zhang, C. H. Foh, and H. Zhang, “Computing and network load balancing for decentralized deep federated learning in industrial cyber-physical systems: A multi-task approach,” *IEEE J. Sel. Areas Commun.*, vol. 43, no. 9, pp. 2997–3013, 2025.
- [16] Y. Ai, Q. Chen, G. Zhu, D. Wen, H. Jiang, J. Zeng, and M. Li, “Clustered federated multi-task learning: A communication-and-computation efficient sparse sharing approach,” *IEEE Trans. Wireless Commun.*, vol. 24, no. 6, pp. 4824–4838, 2025.
- [17] Z. Wang, K. Huang, and Y. C. Eldar, “Spectrum breathing: Protecting over-the-air federated learning against interference,” *IEEE Trans. Wireless Commun.*, vol. 23, no. 8, pp. 10 058–10 071, 2024.
- [18] A. Elbakary, C. B. Issaid, T. ElBatt, K. Seddik, and M. Bennis, “Mira: A method of federated multi-task learning for large language models,” *IEEE Networking Lett.*, pp. 1–1, 2025.
- [19] W. Ni, H. Sun, H. Ao, and H. Tian, “Federated intelligence: When large AI models meet federated fine-tuning and collaborative reasoning at the network edge,” *IEEE Internet Things Mag.*, pp. 1–8, 2025.
- [20] J. Zhang, S. Vahidian, M. Kuo, C. Li, R. Zhang, T. Yu, G. Wang, and Y. Chen, “Towards building the federatedgpt: Federated instruction tuning,” in *Proc. IEEE Int. Conf. Acoust., Speech Signal Process. (ICASSP)*, 2024, pp. 6915–6919.
- [21] R. Ye, W. Wang, J. Chai, D. Li, Z. Li, Y. Xu, Y. Du, Y. Wang, and S. Chen, “Openfedllm: Training large language models on decentralized private data via federated learning,” in *Proc. ACM SIGKDD Conf. Knowl. Discov. Data Min.*, 2024, pp. 6137–6147.
- [22] J. Liu, Y. Liao, H. Xu, and Y. Xu, “Resource-efficient federated fine-tuning large language models for heterogeneous data,” *arXiv preprint arXiv:2503.21213*, 2025.
- [23] Y. Sun, Z. Li, Y. Li, and B. Ding, “Improving LoRA in privacy-preserving federated learning,” in *Proc. Int. Conf. Learn. Represent. (ICLR)*, 2024.
- [24] S. Babakniya, A. Elkordy, Y. Ezzeldin, Q. Liu, K.-B. Song, M. EL-Khamy, and S. Avestimehr, “SLoRA: Federated parameter efficient fine-tuning of language models,” in *Proc. NeurIPS Workshop*, 2023.
- [25] Z. Wang, Y. Zhou, Y. Shi, and K. B. Letaief, “Federated fine-tuning for pre-trained foundation models over wireless networks,” *IEEE Trans. Wireless Commun.*, vol. 24, no. 4, pp. 3450–3464, 2025.
- [26] Q. Zhang, M. Chen, A. Bukharin, P. He, Y. Cheng, W. Chen, and T. Zhao, “Adaptive budget allocation for parameter-efficient fine-tuning,” in *Proc. Int. Conf. Learn. Represent. (ICLR)*, 2023.
- [27] D. Wen, K.-J. Jeon, and K. Huang, “Federated dropout—a simple approach for enabling federated learning on resource constrained devices,” *IEEE Wireless Commun. Lett.*, vol. 11, no. 5, pp. 923–927, 2022.
- [28] S. Xie, D. Wen, X. Liu, C. You, T. Ratnarajah, and K. Huang, “Federated dropout: Convergence analysis and resource allocation,” *arXiv preprint arXiv:2501.00379*, 2024.
- [29] Y. Lin, X. Ma, X. Chu, Y. Jin, Z. Yang, Y. Wang, and H. Mei, “LoRA dropout as a sparsity regularizer for overfitting control,” *arXiv preprint arXiv:2404.09610*, 2024.
- [30] M. Zhu, A. Mao, J. Liu, and Y. Yuan, “Deer: Deviation eliminating and noise regulating for privacy-preserving federated low-rank adaptation,” *IEEE Trans. Med. Imaging*, vol. 44, no. 4, pp. 1783–1795, 2025.
- [31] Y. J. Cho, L. Liu, Z. Xu, A. Fahrezi, M. Barnes, and G. Joshi, “Heterogeneous LoRA for federated fine-tuning of on-device foundation models,” in *Proc. NeurIPS Workshop*, 2023.
- [32] N. Srivastava, G. Hinton, A. Krizhevsky, I. Sutskever, and R. Salakhutdinov, “Dropout: a simple way to prevent neural networks from overfitting,” *J. Mach. Learn. Res.*, vol. 15, no. 1, pp. 1929–1958, 2014.
- [33] Z. Charles and D. Papailiopoulos, “Stability and generalization of learning algorithms that converge to global optima,” in *Proc. Int. Conf. Mach. Learn. (ICLR)*, 2018, pp. 745–754.
- [34] O. Bousquet and A. Elisseeff, “Stability and generalization,” *J. Mach. Learn. Res.*, vol. 2, pp. 499–526, 2002.
- [35] Z. Fu, H. Yang, A. M.-C. So, W. Lam, L. Bing, and N. Collier, “On the effectiveness of parameter-efficient fine-tuning,” in *Proc. AAAI Conf. Artif. Intell. (AAAI)*, vol. 37, no. 11, 2023, pp. 12 799–12 807.
- [36] Y. Yang, D. P. Wipf *et al.*, “Transformers from an optimization perspective,” in *Proc. Conf. Neural Inf. Process. Syst. (NeurIPS)*, vol. 35, 2022, pp. 36 958–36 971.
- [37] H. Sun, H. Tian, W. Ni, J. Zheng, D. Niyato, and P. Zhang, “Federated low-rank adaptation for large models fine-tuning over wireless networks,” *IEEE Trans. Wireless Commun.*, vol. 24, no. 1, pp. 659–675, 2025.
- [38] D. Wen, K.-J. Jeon, M. Bennis, and K. Huang, “Adaptive subcarrier, parameter, and power allocation for partitioned edge learning over broadband channels,” *IEEE Trans. Wireless Commun.*, vol. 20, no. 12, pp. 8348–8361, 2021.
- [39] C. You, K. Huang, H. Chae, and B.-H. Kim, “Energy-efficient resource allocation for mobile-edge computation offloading,” *IEEE Trans. Wireless Commun.*, vol. 16, no. 3, pp. 1397–1411, 2017.
- [40] D. Li, X. Sun *et al.*, *Nonlinear integer programming*. Springer, 2006, vol. 84.
- [41] J. Liu, K. Xiong, D. W. K. Ng, P. Fan, Z. Zhong, and K. B. Letaief, “Max-min energy balance in wireless-powered hierarchical fog-cloud computing networks,” *IEEE Trans. Wireless Commun.*, vol. 19, no. 11, pp. 7064–7080, 2020.
- [42] R. Singhal, K. Ponkshe, and P. Vepakomma, “Exact aggregation for federated and efficient fine-tuning of foundation models,” *arXiv preprint arXiv:2410.09432*, 2024.
- [43] F. Lai, Y. Dai, S. Singapuram, J. Liu, X. Zhu, H. Madhyastha, and M. Chowdhury, “Fedscale: Benchmarking model and system performance of federated learning at scale,” in *Proc. Int. Conf. Mach. Learn. (ICML)*, 2022, pp. 11 814–11 827.